Department
of
APPLIED MATHEMATICS

Effects of bottom drag and shelf slope steepnes on the currents along the shelf slope at Ormen Lange

by

Agathe Sørflaten[1], Jarle Berntsen[1] and Guttorm Alendal[2]

Report no. 164 December 2001

UNIVERSITY OF BERGEN
Bergen, Norway

Department of Mathematics
University of Bergen
5008 Bergen
Norway

ISSN 0084-778X

Effects of bottom drag and shelf slope steepnes on the currents along the shelf slope at Ormen Lange

by

Agathe Sørflaten[1], Jarle Berntsen[1] and Guttorm Alendal[2]

[1]*Mathematical Institute, University of Bergen.*
[2]*Nansen Environmental and Remote Sensing Center, Bergen, Norway*

Report no. 164

December 2001

Effects of bottom drag and shelf slope steepness on the currents along the shelf slope at Ormen Lange

Agathe Sørflaten[1], Jarle Berntsen[1] and Guttorm Alendal[2]

[1] *Department of Mathematics, University of Bergen,Norway*

[2] *Nansen Environmental and Remote Sensing Center, Bergen, Norway*

December 21, 2001

Executive summary

An ongoing acquisition program at Ormen Lange, an offshore gas field located in the Storegga region off mid-Norway, has identified several events in which the currents close to seabed exhibit a short peak value in their speed along with a peak in temperature. This may cause problems with near seabed installations needed for exploration of the gas field. It is therefore essential to understand the generation mechanisms behind these events and to investigate the possibility of forecasting them.

Mean temporal circulation at OL is strongly dominated by the Norwegian Atlantic Current. Tidal effects are weak. The extreme events are driven by strong pressure gradients. That is, strong atmospheric low pressures and/or internal pressure fronts between warmer Atlantic Water and colder Norwegian Sea Water. Along the shelf slope at OL we may get steepening of the iso-surfaces of density, separating AW and NSW, due to strong Ekman veering during storms or approaching internal density fronts. During such events the density surfaces tend to undershoot their equilibrium level, and as the forcing weakens, the suppressed water may run up along the shelf slope. In this run up phase peak values in the velocities are often found.

Since the atmospheric forcing is a major forcing mechanism behind the observed events, it would be of interest to investigate the response of atmospheric low pressures on the currents along the shelf slope at Ormen Lange. Of particular interest is the vertical displacements of different density surfaces at the shelf and the shelf slope. The sensitivity of the near sea bed velocities at Ormen Lange to the bottom drag and the shelf slope factor is studied.

The results show that the velocities reach maxima a few hours after the pressure disturbance force is turned off. The maximum velocity at different locations close to shelf slope is strongest when there is no bottom drag. The iso-surfaces are undershooting their equilibrium levels and as the forcing weakens buoyancy forces create vertical oscillations. It is demonstrated that bottom drag has a significant effect on how the water masses move up and down the slope close to the sea bed during these oscillations. In particular the front of the water masses is found at the bottom when there is no drag, whereas the corresponding front is found some distance above the bottom when effects of bottom drag are included. The maximum velocities reported in the present study are fairly robust to variations in the slope angle.

1 Introduction

Ormen Lange is an offshore gas field located in the Storegga region off mid-Norway in water depths from approximately 800m to 1100m. The field, presently being considered for development under the leadership of Norsk Hydro, is located in the core of the Storegga slide that left a headwall at the shelf break of close to 300 km length. Extracting and transporting gas from the reservoir includes seabed pipeline tracks which makes it essential to know the maximum velocities in the region. This report will focus on near seabed dynamics, as the pipelines are located here.

The water masses in the region may be divided into four different layers classified by their origin, where the depth of the interfaces may vary both in time and space (Hopkins 1990) :

- Norwegian Coastal Water (NCW) on shelf with salinity 32 - 35 p.s.u. and temperature 2 - 13°C due to inflow from the Baltic and runoff from Norwegian rivers,
- Atlantic Water (AW) off shelf with salinity above 35.0 p.s.u. and temperature above 2°C,
- Norwegian Sea Artic Intermediate Water (NSAIW) with salinity below 34.9 p.s.u. and temperature between -0.5 and 0.5°C,
- Norwegian Sea Deep Water (NSDW) with salinity 34.91 p.s.u. and temperature less than 0.5°C,

The different layers are presented in Figure 1 and Table 1. The upper layer of warm and salt AW interface with the cold and fresher NSAIW at around 400 to 600m and rises towards the west. The NSDW is located below 800m and the separation depth increases northwards. The different water masses give rise to strong density fronts (horizontally and vertically) along which a wide range of wave and meandering phenomena may occur. The water masses of the upper layer are subject to significant variations due to atmospheric forcing and has a significant directional variability and maximum velocities above $1ms^{-1}$. The water masses below are clearly more stable and mean direction aligns with large scale bottom topography, flowing with an average speed of 20 to $30cms^{-1}$. Water masses close to the seabed are more directional unstable than the water masses above, and the average velocities are smaller in magnitude. However, intermittent events of short term peaks in velocities and abrupt changes in temperature are observed close to the seabed and described/discussed in Eliassen et al.(2001), Mathisen et al.(2000) and Vikebø et al.(2001). Also, Engedahl & Røed(1999) and

Eliassen & Berntsen(2000) have studied local dynamics using ocean models. At Ormen Lange, one may expect both atmospheric forcing exerted on the upper ocean and mesoscale topography to influence the flow (Legutke 1991).

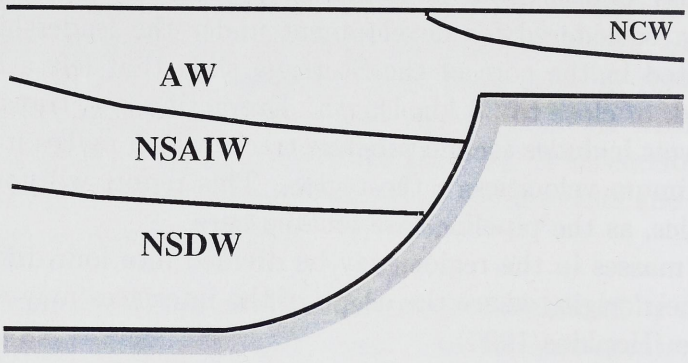

Figure 1: **The water masses in the region divided into four different layers; Norwegian Coastal Water (NCW), Atlantic Water (AW), Norwegian Sea Artic Intermediate Water (NSAIW) and Norwegian Sea Deep Water (NSDW).**

LAYER	S [p.s.u]	T [^{o}C]
NCW	$32.00 - 35.00$	$2.0 - 13.0$
AW	> 35.00	> 2.0
NSAIW	< 34.90	$-0.5 - 0.5$
NSDW	34.91	< 0.5

Table 1: **Salinity and temperature of the layers presented in Figure 1.**

The shelf edge and the slope down into the deep ocean exhibit a vast number of dynamical processes that exceed any other areas in the oceans

Cyclonic wind around a storm centre induces Ekman transport away from the low pressure centre with a subsequent lowering of the surface, though this is partly compensated by an elevation of the surface due to a lower atmospheric pressure. The water is transported away from the low pressure centre giving rise to an upward Ekman transport, Ekman-pumping. This causes a transport away from the storm centre in the upper layer and towards it in the deeper water masses. At Ormen Lange the oscillations and transports away from and towards storm centres passing by in the Nordic Seas result in water moving down the shelf slope, Figure 2a). This downwelling increases

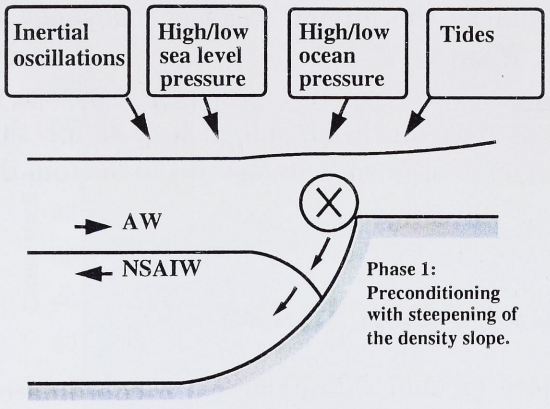

(a)

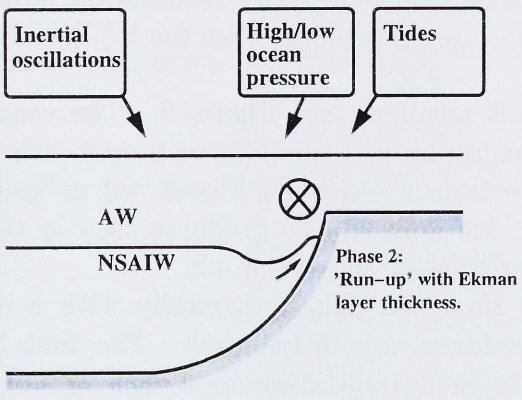

(b)

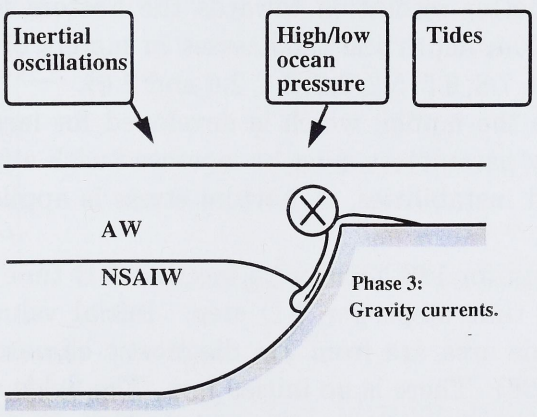

(c)

Figure 2: . **A plausible model explaining the effect on the currents at Ormen Lange of a low pressure disturbances in the Nordic waters.**

the temperature near the seabed. The watermasses will undershoot their equilibrium levels and as the forcing weakens buoyancy forces will create vertical oscillations, Figure 2b) and c). In this paper effects of atmospheric low pressures on the oscillations of the density surfaces and near bottom currents are studied. An idealized model is used for this purpose. The sensitivity of the currents at Ormen Lange to the bottom drag and the slope factor of the shelf are investigated.

2 Numerical experiment

The system of equations and the numerical σ-coordinate ocean model are described in Berntsen (2000). The equations are the continuity equation for an incompressible fluid, the Reynolds averaged momentum equations horizontally, in the vertical the hydrostatic assumption is made, conservation equations for temperature and salinity and the UNESCO-equation of state, see Gill (1982).

The model area is idealized, see Figure 3. The coastline is at $y = 0$ and the bottom topography is a function of y only. The depth profile for the Ormen Lange section is shown in Figure 4a) as given by Gjevik and Ommundsen(2000). An approximate profile is used in the experiment, see Figure 4b), which is described in section 4.2.

The grid size is 25×101 cells horizontally with a resolution of 2km. In the vertical 45 σ-layers are distributed. The first 35 layers are distributed according to a formula given in Lynch et al.(1995). Their formula distribute the layers symmetricly about the midpoint and such that we get gradually a finer resolution towards the surface. The last 10 layers give an even better resolution towards the bottom than the Lynch et al.formula. At 1300m depth the thicknesses in meters of the last 10 layers are (16.9, 13.0, 10.4, 7.8, 6.5, 5.2, 3.9, 2.6, 2.6 and 2.6).

In order to use the model, which is developed for large scale problems, horizontal viscosity parameters must be increased with a factor 50 to 100, to avoid checkerboard instabilities. A bottom stress is applied as described in section 4.1.

The model is run for 120 hours with internal 3-D time step equal to 60s. There are 32 2-D time steps per 3-D step. Initial values of temperature and salinity for this area are from the diagnostic climatology described in Engedahl et al.(1998). There is no initial flow. The fields are depth varying, but set to be horizontally constant. Vertical profiles of temperature, salinity, density and the buoyancy frequency are given in Figure 5.

At the lateral open boundaries, periodic confinements are used along the

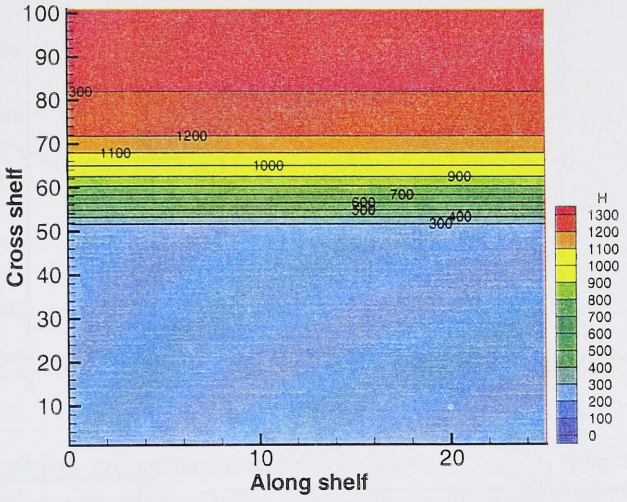

Figure 3: The model area. Colour coding for depth in meters.

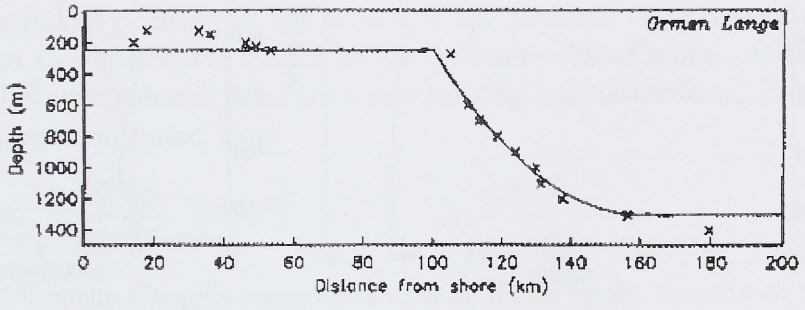

(a)

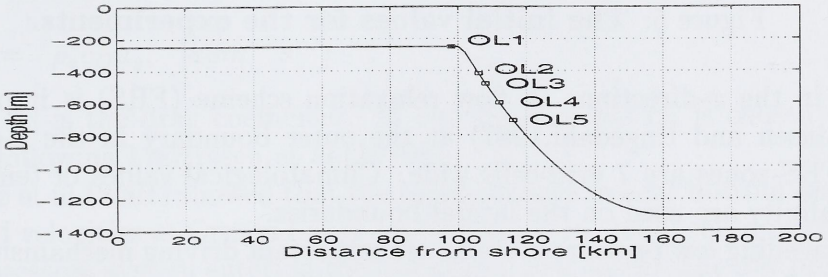

(b)

Figure 4: Depth profile for the Ormen Lange section, Gjevik and Ommundsen(2000).a) The depth read from map marked with crosses. Full drawn line parabolic profile.b) The depth profile with the locations OL1-OL5 used in the studies.

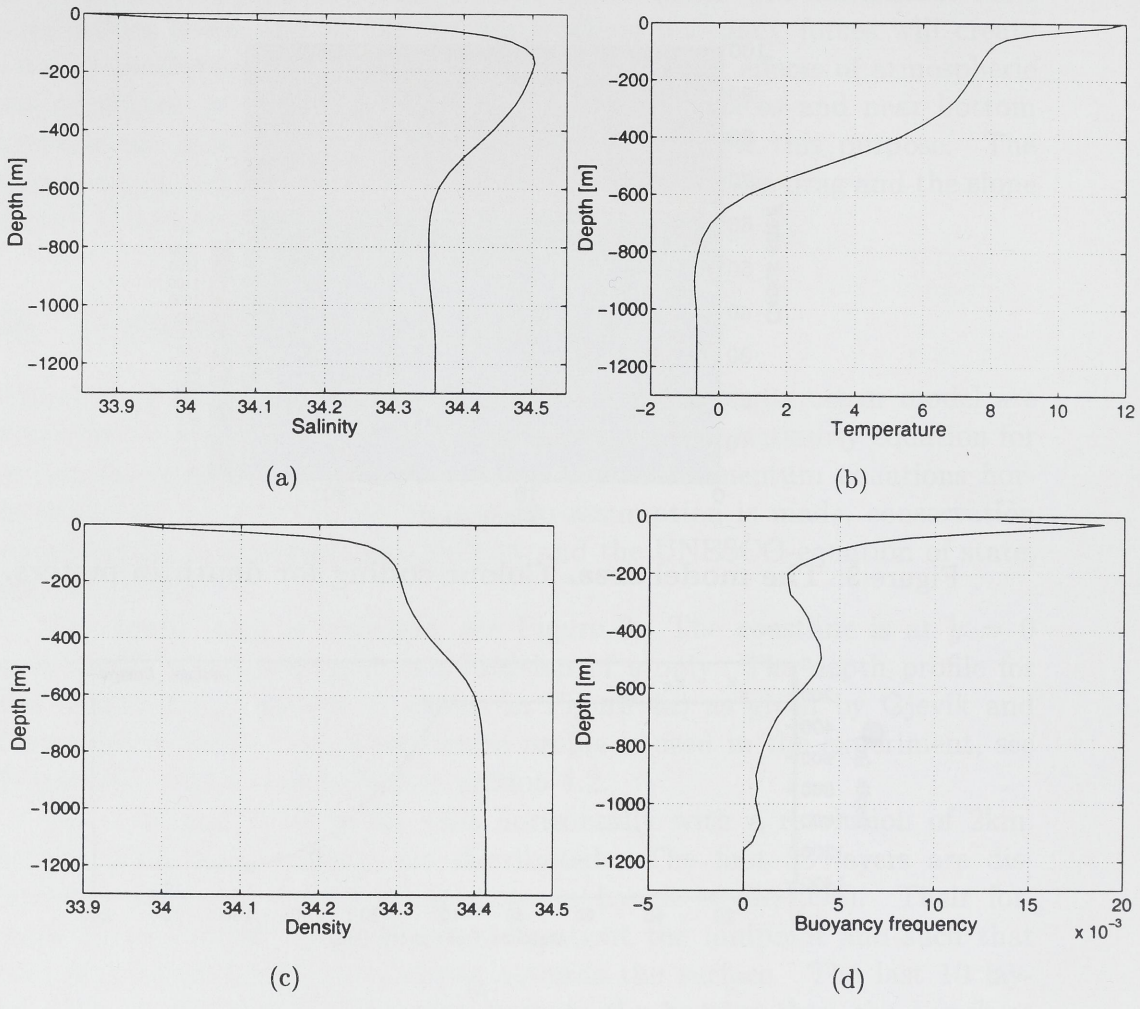

Figure 5: **The initial values for the experiments.**

shelf, in the x-direction. A flow relaxation scheme (FRS) is implemented (Martinsen and Engedahl,1987) at the outer boundary in the y-direction. The FRS-zones are 7 grid-cells wide. Climatological values of temperature and salinity are used on the lateral boundaries.

Travelling low pressure systems are important driving mechanisms for the oceanic flow. Martinsen et al.(1979) constructed an analytical model for a cyclone and studied barotropic effects of the moving cyclone. The atmospheric pressure disturbance is described by, following Martinsen et al.(1979),

$$p(y,t) = p_0(t)e^{-(y-y_0)^2/R^2}, \quad [Nm^{-2}] \quad , \tag{1}$$

where $p_0(t)$ $[Nm^{-2}]$ is the pressure disturbance at the centre of the cyclone;

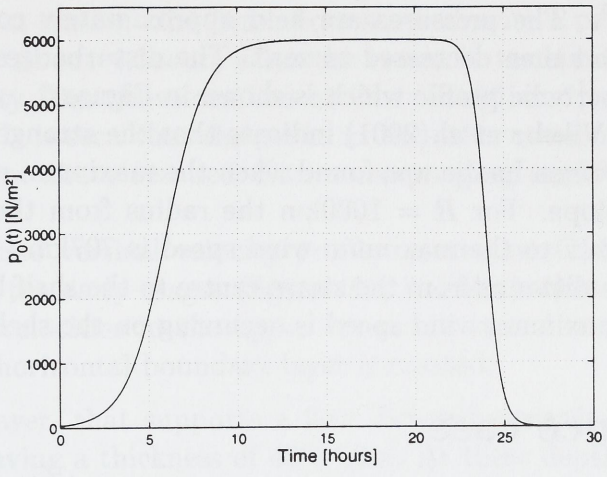

Figure 6: **Time series of pressure disturbance, $p_0(t)$, for the experiments with maximum disturbance equal to 6000Nm^{-2}. The experiments are run for 120hours where $p_0(t) = 0$ for $t > 30$hours.**

y_0 $[km]$ the initial position of the centre of the pressure disturbance and R $[km]$ defines the horizontal extent of the pressure disturbance. From gradients in the atmospheric pressure wind velocity components u_g $[ms^{-1}]$ in x-direction, are computed from

$$u_g = -\frac{0.7}{f\rho_a}\frac{\partial p}{\partial y}, \quad [ms^{-1}] \quad , \tag{2}$$

where f $[s^{-1}]$ is the Coriolis parameter and ρ_a $[kgm^{-3}]$ the density of the air ($1.3kgm^{-3}$ has been used).

From the wind velocity components wind stress is computed from

$$\tau_x = \rho_a c_D u_g, \quad [kgm^{-2}s^{-1}] \quad , \tag{3}$$

where c_D [1] is the drag coefficient. In our experiments c_D is chosen to be 3×10^{-3} following Martinsen et al.(1979).

Vikebø et al.(2001) showed that the rapid changes in near bottom temperatures and velocities at Ormen Lange on November 16, 1996, could be related to a low pressure system entering the Norwegian Sea basin. The low pressure system entered close to Greenland and moved with a speed of approximately 9.84 ms^{-1} towards the Barents Sea. Based on weather maps from this period the horizontal extent of the low pressure system was approximately 1000km.

In order to study the numerical response of this low pressure on the flow at Ormen Lange the centre of the low pressures is located at positions $y_0 = 807$km, $R = 1000$km and $p_0(t)$ is increased over the next 12 hours to

about 6000Nm^{-2}. The pressures are held approximately constant for the next 12 hours, and then decreased to zero. The disturbances are described by a tangens hyperbolic profile which is shown in Figure 6.

Results from Vikebø et al.(2001) indicate that the strongest response on the currents at Ormen Lange was found when the maximum wind speed was along the shelf slope. For R = 1000km the radius from the centre of the low pressure system to the maximum wind speed is 707km ($R/\sqrt{2}$). In the present study the distance from the storm centre to the shelf break is 707km indicating that maximum wind speed is occurring on the shelf break.

3 Reference case

This section describes the results of the numerical simulations in a Reference experiment using forcing and model setup as presented in the previous section. The focus will be on local response near the sea bed at OL1-OL5, Figure 4b), with depths as indicated in Table 2. These stations are believed to represent the different areas along the shelf edge and the shelf slope.

Location	OL1	OL2	OL3	OL4	OL5
Depth [m]	267	450	511	627	735

Table 2: **The depth at station OL1-OL5.**

In the experiment inertial oscillations with period of about 13.4hours are induced. Shelf modes with a period of about one day are not appearing due to the short model area applied (Gjevik and Ommundsen (2000)). The short domain also makes along shelf variability negligible in the present studies.

Time series of velocity at stations OL1-OL5, 10m and 50m above sea bed, are shown in Figure 8a) and b). The velocities increase as long the pressure disturbance force is on, reaching a maxima a few hours after the force is set to zero, whereupon damped oscillations occur. Similar patterns are seen in the temperature time series in Figure 8c) and d). An exception is the station OL1 close to shelf break, 10m and 50m above sea bed, where the temperatures stay approximately constant throughout the event. It is worth noticing the larger damping in the shallowest stations in Figure 8a) and b) compared to the deeper ones. This is probably because they exhibit larger velocities and thus larger friction and energy drain. At the deeper stations the oscillations are less damped after the storm is terminated.

Table 4 shows the maximum velocities and time of occurrence at OL1-OL5, 10m and 50m above sea bed. Maximum velocity among the investigated

depths is found at station OL1 50m above sea bed, with a peak of $0.290 ms^{-1}$ after 28.5hours, about 4.5hours after the storm is terminated. The corresponding velocity 10m above sea bed at OL1 is $0.261 ms^{-1}$, and takes place one hour later. It is seen that the peaks at the other stations are larger and occur earlier 50m above sea bed than corresponding peaks 10m above sea bed.

Figure 9 shows vertical velocity profiles at station OL3 from $t = 20$h to $t = 30$h. In the early stages (figures 9a, b and c) when wind forcing is increasing, the velocities in the upper layers are veered to the right of the wind stress. A horizontal boundary layer is created,

i) an Ekman layer, that supports a flow directed towards the coast. The layer is having a thickness of $40 - 50$m. At these depths the tip of the velocity vectors during the period trace out a curve that looks like an Ekman spiral. At the bottom of the layer there is a velocity oriented in the along shelf direction approximately.

ii) In the interior layer the currents do not change notably with depth.

iii) The bottom exerts a stress due to bottom friction against the flow, bringing the velocities to zero in an Ekman layer with thickness of $10 - 15$m above the bottom.

After the wind forcing is turned off (figures 9d, e and f) i) the Ekman layer near the surface is reduced.

The vertical displacements of the 0^oC and 4^oC iso-surfaces are then studied at the stations OL1-OL5. Time series the 4^oC iso-surface are shown in Figure 10a) for OL3 to OL5. When the pressure force is present, the surface is moved deeper. After the force is turned off, the iso-surface is raised at the deepest locations and show an oscillating behaviour during the rest of the event. Similar displacements are seen during the initial phase for the 0^oC iso-surface in Figure 10b) at OL5. However, for this case the oscillatory behavior is absent since the iso-surface is not present at this depth during the rest of the event.

Figure 11 shows maximum and minimum depths for the iso-surfaces. While the wind forcing is present, the minimum is decreasing. As the forcing weakens, the minimum moves upwards. The largest amplitude difference of oscillations for the 4^oC iso-surface is 29m occurring three hours after the pressure forcing is set to zero. The corresponding difference of the 0^oC surface is 18m one hour later. Ekman pumping can explain the described vertical displacements of the different water masses.

The time evolution of velocity v $[ms^{-1}]$ in a vertical cross shelf transect is presented in Figure 12. At the early stages water is transported towards the

shore in the upper layers and the deeper water masses are transported away from the shore. This pattern is due to Ekman transport. After the forcing is terminated, the further evolution shows that water is also transported away from the shelf slope in a thin layer close to sea bed.

In the vertical cross shelf transect in Figure 13 the isotherms for 7.2°C, 6.4°C and 5.6°C are presented. It shows that the layers are undershooting their equilibrium levels during the period from $t = 0$ to $t = 28$h as water moves down the shelf slope. The deepest isotherms display a vertical profile near bottom. Mixing occurs where lighter water is moving under heavier water. For the next six hours, up to $t = 34$h, the suppressed water run up along the shelf slope. The lowering and the raising of the layer 6.4°C coincide with the occurrence of the earliest peak and bottom in temperature at OL2 10m and 50m above seabed in Figure 8c) and d) after the forcing is set to zero. Downwelling and upwelling thus increase and decrease the temperature near the seabed. The further evolution seen in Figure 13 shows that the vertical oscillations are decreasing. Totally the iso-surfaces are lowered. The iso-surfaces for colder water than 5.6°C have similar but smaller vertical oscillations.

4 Sensitivity analysis

Any numerical experiment rely on different assumptions and simplifications. Since the region close to the ocean floor is so important a sensitivity analysis on the bottom friction and the slope factor of the shelf are performed.

4.1 Bottom drag

In the model the bottom stress is described by a quadratic law,

$$\tau_b = \rho_0 C_D |\mathbf{U}_b| \mathbf{U}_b, \quad [Nm^{-2}] \quad , \tag{4}$$

where $\mathbf{U}_b$ $[ms^{-1}]$ is the along shelf velocity component at the bottom. The drag coefficient C_D [1] is given by

$$C_D = \max[0.0025, \frac{\kappa^2}{(\ln(z_b/z_0))^2}], \tag{5}$$

where z_b $[m]$ is the distance of the nearest grid point to the bottom, and the von Karman constant is $\kappa = 0.4$ [1]. In lack of further information the bottom roughness parameter is set to $z_0 = 0.010$m in the Reference case (Weatherly and Martin 1978). The sensitivity of the bottom drag is

studied through three additional experiments as shown in Table 3. In experiment Run_BCD_0 there is no drag, while in the following two experiments, Run_BZ_0.001 and Run_BZ_0.100, the bottom roughness parameter z_0 is set to 0.001m and 0.100m, respectively. The response of the currents at Ormen Lange with focus near the sea bed is then compared to results from the Reference case experiment.

Experiment	z_0
Reference	0.010m
Run_BCD_0	–
Run_BZ0_0.001	0.001m
Run_BZ0_0.100	0.100m

Table 3: **Table of the bottom roughness parameter z_0 in the numerical experiments. The solid line (-) indicates no bottom drag.**

Time series of the velocities at OL1-OL5 10m and 50m above sea bed are presented in Figures 14 and 15 respectively. As for the reference case, the velocities are reaching maxima a few hours after the low pressure force is terminated, whereupon inertial oscillations are seen. Table 4 shows the maximum velocities and time of occurrence at OL1-OL5, 10m and 50m above sea bed. The maximum velocity among the investigated events and depths is found at OL1. Largest velocities are found, as expected, for the case with no bottom drag. No friction also gives, as expected less damping of the oscillations. Also notice the lesser peak in maximum velocity closer to the bottom, except for the shallowest station, for the no friction case.

Figure 16 shows decreasing maximum velocities with increasing values of the bottom roughness parameter at OL1 to OL5. At OL1 the reduction in the velocities with increased bottom drag is greater than at the other locations. This is most obvious 10m above sea bed. The velocities 50m above sea bed are fairly robust to the choice of z_0.

In Figure 17 it is seen how the maximum velocity at OL1-OL5 is reduced with depth. The reduction is largest in experiment Run_BCD_0 and smallest in experiment Run_BZ0_0.100 which is most obvious 10m above sea bed. This can indicate that the reduction in the maximum velocity with depth is decreased with increased bottom drag close to sea bed.

The isotherms for 7.2°C, 6.4°C and 5.6°C are presented in a vertical cross shelf transect for the experiment Run_BCD_0 in Figure 19. In the early stages, up to $t = 28$h, the layers undershoot their equilibrium levels along the shelf slope as in the Reference experiment. The iso-surfaces do not display a

Experiment \Station	OL1	OL2	OL3	OL4	OL5
10m a.s.b.*					
Reference case					
Max speed [ms^{-1}]	0.261	0.138	0.110	0.102	0.093
Time [hour]	27.5	27.0	26.0	25.0	26.0
Run_BCD_0	0.311	0.180	0.151	0.117	0.099
	28.5	28.0	27.5	26.5	27
Run_BZ0_0.001	0.279	0.151	0.132	0.112	0.096
	27.5	27.0	26.0	26.0	27.0
Run_BZ0_0.100	0.226	0.115	0.097	0.091	0.086
	27.0	26.0	25.0	24.5	26.0
50m a.s.b.					
Reference case	0.290	0.192	0.164	0.122	0.100
	28.5	28.0	27.5	27.0	27.0
Run_BCD_0	0.307	0.193	0.164	0.123	0.101
	28.5	28.0	28.0	27.0	27.0
Run_BZ0_0.001	0.295	0.192	0.163	0.122	0.100
	28.5	28.0	28.0	27.0	27.0
Run_BZ0_0.100	0.282	0.194	0.164	0.121	0.099
	28.5	27.5	27.0	27.0	27.0

Table 4: **Maximum velocity at OL1-OL5, 10m and 50m above sea bed *, for different values of the bottom roughness parameter z_0.**

vertical profile close to the bottom. The suppressed water run up along the shelf slope with the head of the iso-surfaces at the bottom during the next six hours. Also in this case the downwelling and the upwelling coincide with the earliest peak and bottom in temperature at OL2, 10m and 50m above sea bed, after the forcing is set to zero in Figure 18. During the event, the lowering of the iso-surfaces is dominating. At greater depths than seen in Figure 19 similar oscillations of layers appear but with smaller amplitudes.

4.2 Slope factor

In the model the shelf slope profile is approximated by a parabolic function Gjevik and Ommundsen(2000),

$$H = \begin{cases} H_s & 0 \leq y \leq S_1 \\ H_0 - (H_0 - H_s)\left(\dfrac{S_2 - y}{S_2 - S_1}\right)^2 & S_1 < y < S_2 \\ H_0 & S_2 \leq y \leq L_y \end{cases} \quad (6)$$

with uniform depths, H_s $[m]$ and H_0 $[m]$, off the shelf slope. The corresponding quantities in the cross shelf direction are S_1 $[km]$ and S_2 $[km]$, respectively. The depth and the width of the shelf slope are determined by $(H_s - H_0)$ $[m]$ and $(S_2 - S_1)$ $[km]$. The constant $L_y = 200$km is the dimension of the model area in the y-direction. The parabolic shelf slope profile is a good approximation particular when the shelf slope is steep. In the Reference experiment the shelf slope is modelled by equation 6 with $H_s = -250$m, $H_0 = -1300$m, $S_1 = 100$km and $S_2 = 160$km, given in Figure 4b). In order to investigate the sensitivity of the near bottom currents at Ormen Lange to the slope factor the width of the shelf slope is modified by adjusting S_1 and S_2. The values of these parameters in four additional experiments are given in Table 5. The values correspond to extensions of the width of the shelf slope with 25%, 50%, 75% and 85%, respectively.

Experiment	S_1	S_2	$(S_2 - S_1)$
Reference	100	160	60
Run_S1S2_1	95	170	75
Run_S1S2_2	88	178	90
Run_S1S2_3	84	189	105
Run_S1S2_4	82	193	111

Table 5: **Table of the parameters S_1 $[km]$ and S_2 $[km]$ determining the width of the shelf slope $(S_2 - S_1)$ $[km]$ in the numerical experiments.**

The different shelf slope profiles are given in Figure 7. The response of the currents are then compared to the results in the Reference experiment. The focus will be on local response near the sea bed at OL1-OL5 with depths in the experiments as indicated in Table 6.

Time series of the velocities, 10 and 50m above sea bed, at OL1-OL5 are given in Figures 20 and 21, respectively. As for the reference case, the velocities are reaching maxima a few hours after the low pressure force is terminated, whereupon inertial oscillations are induced. Table 7 shows the maximum velocities and time of occurrence at OL1-OL5, 10 and 50m above sea bed. The maximum velocity among the investigated events and depths

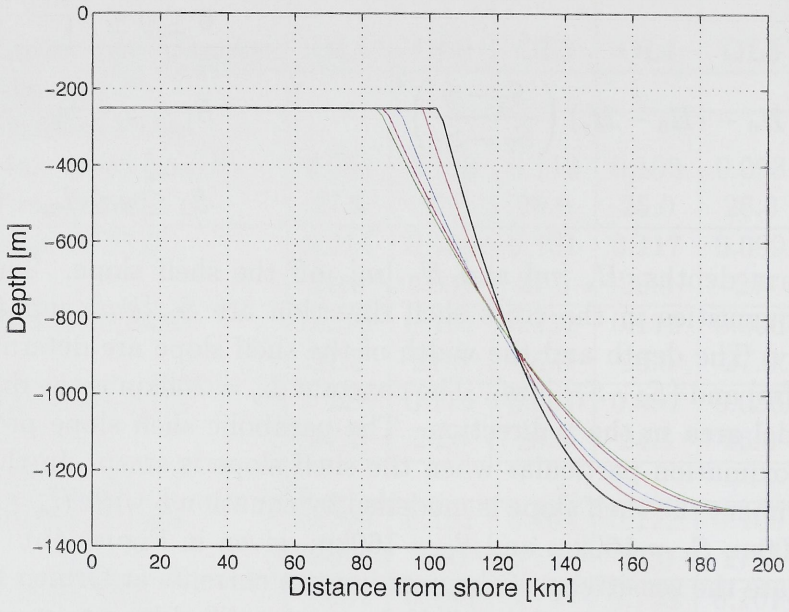

Figure 7: **The depth profile for different shelf widths. The black, red, cyanid, pink and green line represents Reference case, Run_S1S2_1, Run_S1S2_2, Run_S1S2_3 and Run_S1S2_4 experiments, respectively.**

Experiment \Station	OL1	OL2	OL3	OL4	OL5
Reference case Depth [m]	267	450	511	627	735
Run_S1S2_1	278	437	535	628	755
Run_S1S2_2	296	428	511	628	735
Run_S1S2_3	290	440	511	612	735
Run_S1S2_4	287	431	531	625	741

Table 6: **The depths at station OL1-OL5 for different widths of the shelf slope.**

is found at OL1. The velocity is smaller than in the Reference case. This may be caused by the deeper location of OL1 in the Run_S1S2 experiments as indicated in Table 6. Largest velocities are found in the case with widest shelf slope. At the deeper stations the maximum velocities are larger when the width of the slope is extended. It is worth noticing that the majority of the stations OL3-OL5 in the events Run_S1S2 are located deeper than in the Reference case in Table 6.

Experiment \Station	OL1	OL2	OL3	OL4	OL5
10m a.s.b.*					
Reference case					
Max speed [ms^{-1}]	0.261	0.138	0.110	0.102	0.093
Time [hour]	27.5	27.0	26.0	25.0	26.0
Run_S1S2_1	0.249	0.154	0.122	0.110	0.098
	27.0	27.0	26.0	25.5	26.5
Run_S1S2_2	0.247	0.165	0.134	0.117	0.104
	27.0	27.0	26.0	26.0	26.5
Run_S1S2_3	0.254	0.163	0.140	0.122	0.104
	27.0	27.0	26.0	26.0	27.0
Run_S1S2_4	0.256	0.170	0.135	0.120	0.103
	27.0	26.5	27.0	26.5	27.0
50m a.s.b.					
Reference case	0.290	0.192	0.164	0.122	0.100
	28.5	28.0	27.5	27.0	27.0
Run_S1S2_1	0.282	0.202	0.158	0.127	0.102
	28.0	28.0	27.5	27.0	27.0
Run_S1S2_2	0.281	0.211	0.172	0.130	0.108
	28.0	28.0	28.0	27.0	28.0
Run_S1S2_3	0.287	0.205	0.173	0.136	0.108
	28.0	28.0	28.0	27.5	28.0
Run_S1S2_4	0.289	0.209	0.164	0.131	0.106
	28.0	28.0	28.0	28.0	28.0

Table 7: **Maximum velocity at OL1-OL5, 10m and 50m above sea bed *, for different values of the parameters S_1 and S_2.**

The isotherms for 7.2°C, 6.4°C and 5.6°C in a vertical cross shelf transect for the experiment Run_S1S2_4 are given in Figure 23. It is seen that the layers are undershooting their equilibrium levels up to $t = 28$h. The deepest isotherms display a vertical profile near bottom as in the Reference case. The suppressed water run up along the shelf slope during the next six hours. In this case too the downwelling and the upwelling coincide with the earliest peak and bottom in temperature at station OL2, 10m and 50m above sea bed, after the forcing is terminated in Figure 22. Totally the layers are lowered. The iso-surfaces for colder water than 5.6°C have similar but smaller vertical oscillations.

5 Conclusions

The response of atmospheric low pressures on the currents along the shelf slope at Ormen Lange is studied. The studies include a sensitivity analysis for the dynamics close to the sea bed for varying bottom drag and shelf slope. An idealized model is used for this purpose and with a model domain too short to include shelf modes.

All the different numerical studies show the same general features; The currents velocities reach maxima a few hours after the pressure disturbance force is turned off followed by damped inertial oscillations. Further the results reveal Ekman dynamics in the area; A boundary layer is created near the surface where the velocities display an Ekman spiral. At the bottom a similar, although thinner layer, is created. It is also seen that at early stages water is transported towards shore in the upper layer and away from the shore and the shelf slope in the deeper water masses. The transport results in water moving down the shelf slope with an associated lowering of temperature layers. As the wind forcing weakens the suppressed water run back up along the shelf slope, overshoot, and create damped vertical oscillations. Totally the iso-surfaces are undershooting their equilibrium levels.

The bottom drag sensitivity study show that, as expected, the maximum velocity at different locations close to shelf slope is strongest when the drag is absent. It has also been shown that the velocities decrease significantly close to shelf break with increasing drag. This is because the largest current velocities are found at this location and hence are more influenced by the drag. The velocities 50m above sea bed are fairly robust to the choice of bottom roughness parameter z_0 indicating that bottom drag has highest influence on the current velocity close to the sea bed. The results show that including bottom drag creates a more vertical profile of the density surfaces close to bottom. This indicates that the drag will affect the transport of water masses close to sea bed.

The sensitivity analysis on the slope factor of the shelf show that at deeper water levels close to bottom the maximum velocity is increased when the width of the shelf slope is extended. The majority of the level depths are located deeper than in the Reference case, indicating that extension of the shelf slope in the cross shelf direction influences the velocity close to sea bed. Further the experiments show that the vertical oscillations and hence the transport close to bottom are almost unaffected by extension of width of the shelf slope.

In the present studies the maximum values of the current velocities are smaller than Vikebø et al.(2001) showed in their studies. This may be caused by the exclusion of Atlantic inflow and shelf modes.

This study reveal the importance of proper bottom drag parameterization in fluid models for accurate simulations of transport and currents on a shelf and a continental slope. The study has been made using a simplified topography. The importance of proper drag inclusion becomes even more important if realistic topography is used.

Acknowledgements This work has been supported by Norsk Hydro grant NHT-B44-5098606-00.

References

Berntsen, J. (2000), USERS GUIDE for a modesplit σ-coordinate numerical ocean model, Technical Report 135, Dept. of Applied Mathematics, University of Bergen, Johs. Bruns gt.12, N-5008 Bergen, Norway. 48p.

Eliassen, I. & Berntsen, J. (2000), 'Evaluation of methods for estimating the internal pressure in sigma-coordinate ocean models using measurements from the Norwegian trench and the Skagerrak'. Manuscript, Department of Mathematics, University of Bergen.

Eliassen, I. K., Eldevik, T., Berntsen, J. & Furnes, G. (2000), 'The current conditions at the Ormen Lange-Storegga'. Manuscript, Department of Mathematics, University of Bergen.

Engedahl, H., Ådlandsvik, B. & Martinsen, E. (1998), 'Production of monthly mean climatological archives of salinity, temperature, current and sea level for the Nordic Seas', *J. Mar. Syst.* **14**, 1–26.

Engedahl, H. & Røed, L. P. (1999), 'Forecasting ocean currents in deep water areas: the Ormen Lange case', *DNMI Reseach Report No. 80, Norwegian Meteorological Institute* .

Gill, A. (1982), *Atmosphere-Ocean Dynamics*, Academic Press. ISBN-0-12-283520-4.

Hopkins, C. & Nilssen, E. (1990), The rise and fall of the Barents Sea capelin, *in* E. Sakshaug, C. Hopkins & N. Øritsland, eds, 'Proceedings of the Pro Mare Symposium on Polar Marine Ecology', Polar Research -10.

Legutke, S. (1991), 'A numerical investigation of the circulation in the Greenland and Norwegian seas', *J. Phys. Oceanogr., 21* pp. 118–148.

Lynch, D., Ip, J., Naimie, C. & Werner, F. (1995), Convergence studies of tidally-rectified circulation on Georges Bank, *in* D. Lynch & A. Davies, eds, 'Quantitative Skill Assessment for Coastal Ocean Models', American Geophysical Union.

Martinsen, E. & Engedahl, H. (1987), 'Implementation and testing of a lateral boundary scheme as an open boundary condition in a barotropic ocean model', *Coastal Engineering* **11**, 603–627.

Martinsen, E., Gjevik, B. & Røed, L. (1979), 'A numerical model for long barotropic waves and storm surges along the western coast of Norway', *J.Phys.Oceanogr.* **9**, 1126–1138.

Mathisen, J. P., Hackett, B. & Engerdahl, H. (2000), 'Description of special current events using observed and simulated data', *OCEANOR report OCN R-99022* .

Ommundsen, A. & Gjevik, B. (2000), Scattering of tidal Kelvin waves along shelves which vary in their lengthwise direction, *in* A. Ommundsen, ed., 'Numerical simulations of tides, shelf slope currents and Lagrangian advection of particles', Unipub, Oslo.

Vikebø, F. B., Berntsen, J. & Furnes, G. K. (2001), 'Analysis of measurements at Ormen Lange', *Tech. rep., Dept. of Applied Mathematics, University of Bergen* .

Weatherly, G. & Martin, P. (1978), 'On the structure and dynamics of the ocean bottom boundary', *J. Phys. Oceanogr.* **8**, 557–570.

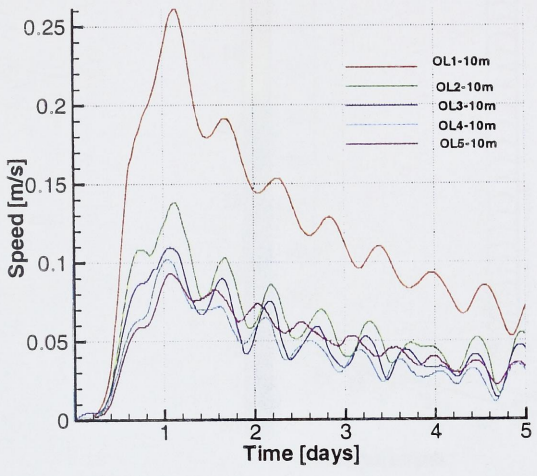

(a) **Velocity 10m a.s.b.***

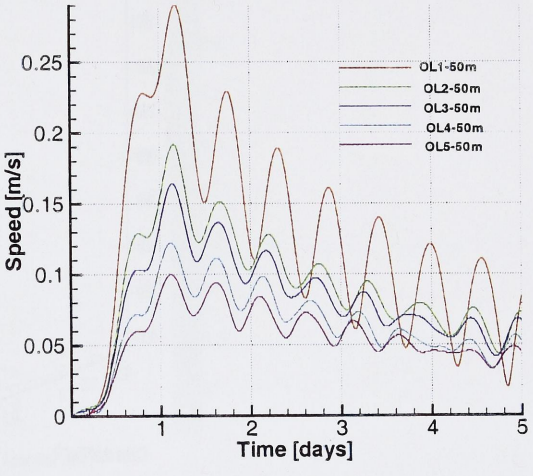

(b) **Velocity 50m a.s.b.**

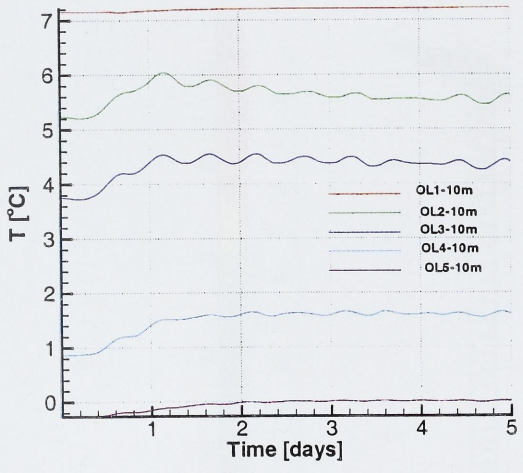

(c) **Temperature 10m a.s.b.**

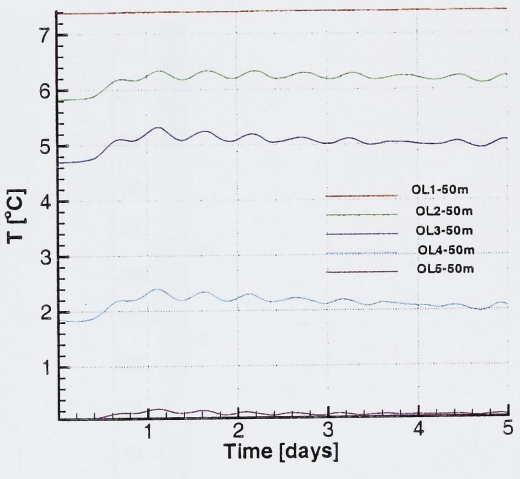

(d) **Temperature 50m a.s.b.**

Figure 8: **The velocity and the temperature 10m and 50m above sea bed* at OL1-OL5 for the Reference experiment.**

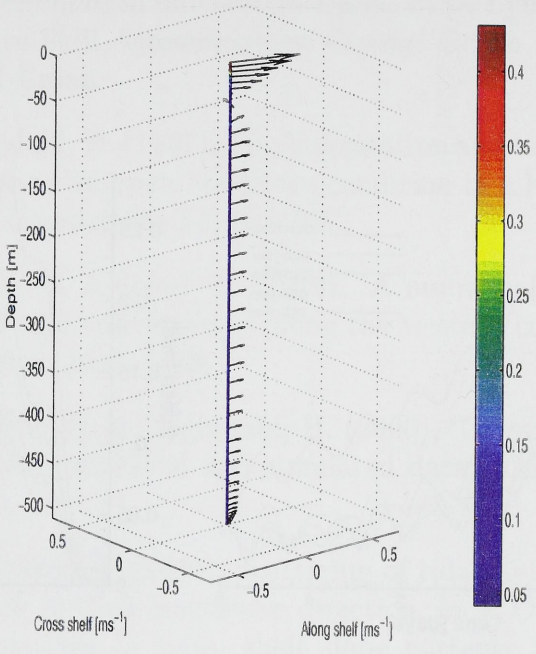
Depth [m]
0
-50
-100
-150
-200
-250
-300
-350
-400
-450
-500
0.5
0
-0.5
Cross shelf [ms^{-1}]
-0.5
0
0.5
Along shelf [ms^{-1}]
0.4
0.35
0.3
0.25
0.2
0.15
0.1
0.05

(a) **t=20h**

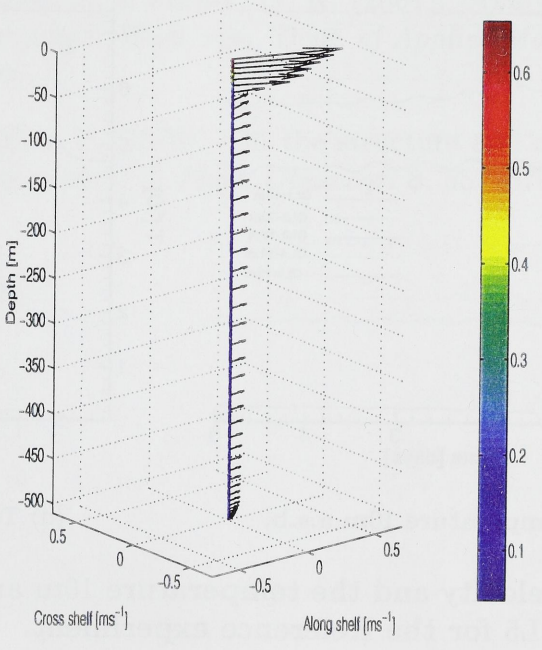
Depth [m]
0
-50
-100
-150
-200
-250
-300
-350
-400
-450
-500
0.5
0
-0.5
Cross shelf [ms^{-1}]
-0.5
0
0.5
Along shelf [ms^{-1}]
0.6
0.5
0.4
0.3
0.2
0.1

(b) **t=22h**

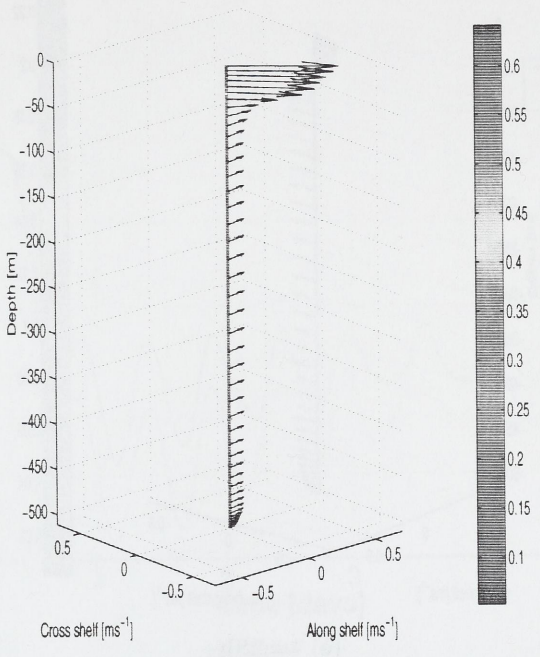
Depth [m]
0
-50
-100
-150
-200
-250
-300
-350
-400
-450
-500
0.5
0
-0.5
Cross shelf [ms^{-1}]
-0.5
0
0.5
Along shelf [ms^{-1}]
0.6
0.55
0.5
0.45
0.4
0.35
0.3
0.25
0.2
0.15
0.1

(c) **t=24h**

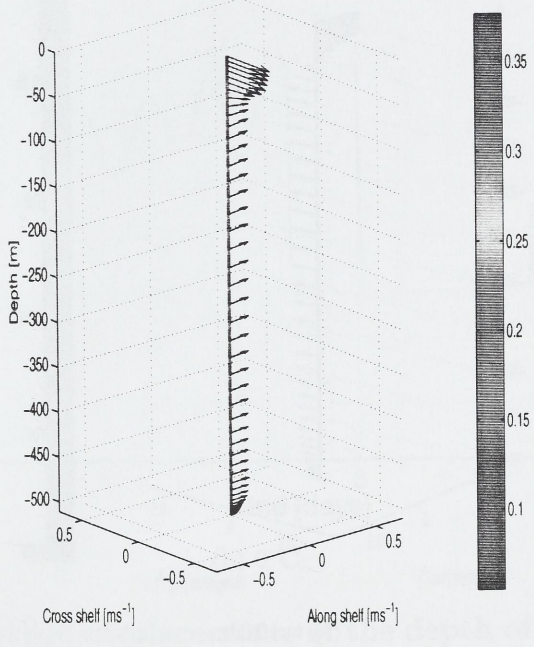
Depth [m]
0
-50
-100
-150
-200
-250
-300
-350
-400
-450
-500
0.5
0
-0.5
Cross shelf [ms^{-1}]
-0.5
0
0.5
Along shelf [ms^{-1}]
0.35
0.3
0.25
0.2
0.15
0.1

(d) **t=26h**

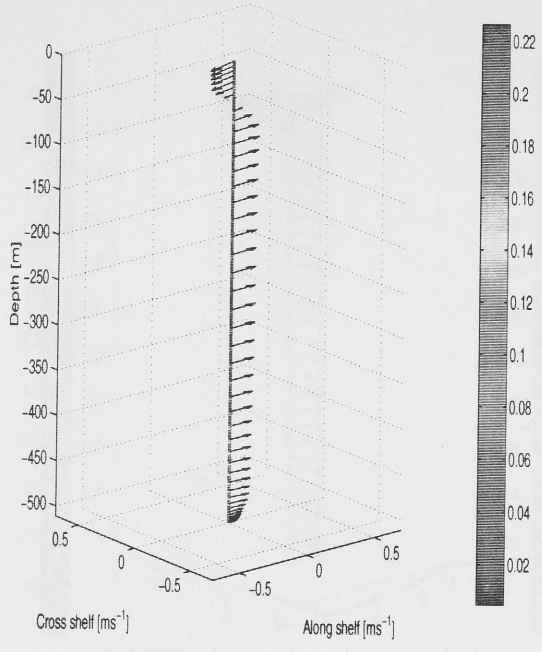

(e) **t=28h**

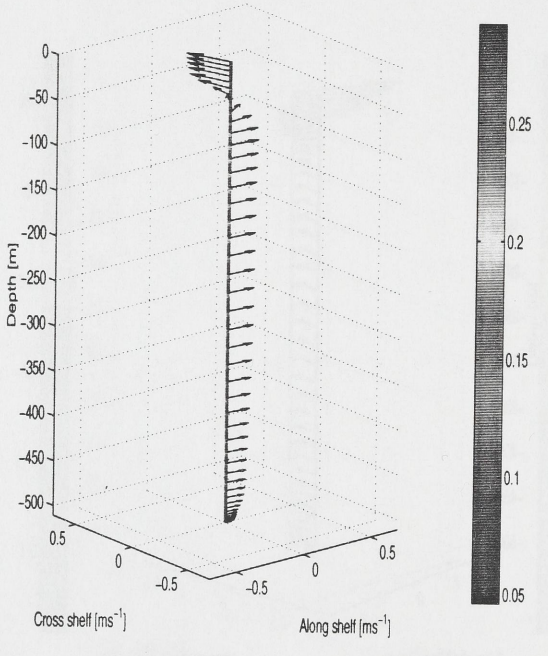

(f) **t=30h**

Figure 9: **The velocity profile at station OL3 during the period from $t = 20$h to $t = 30$h for the Reference experiment.**

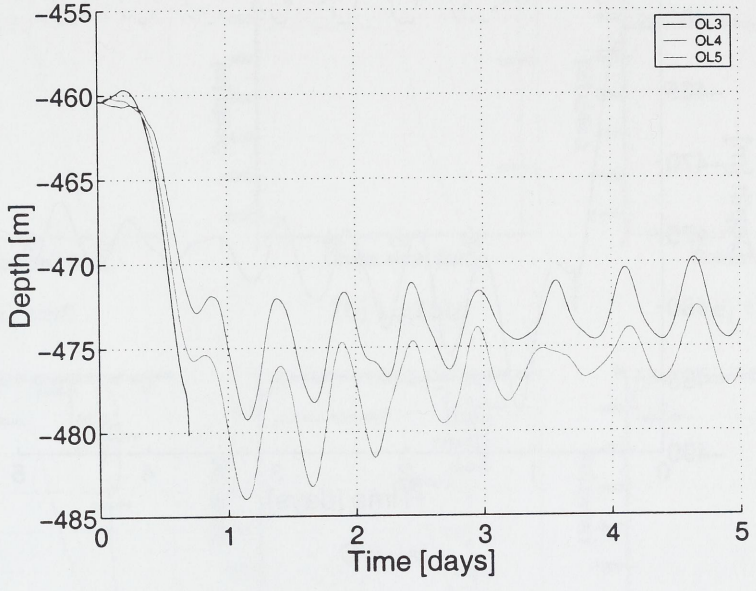

(a) 4°C

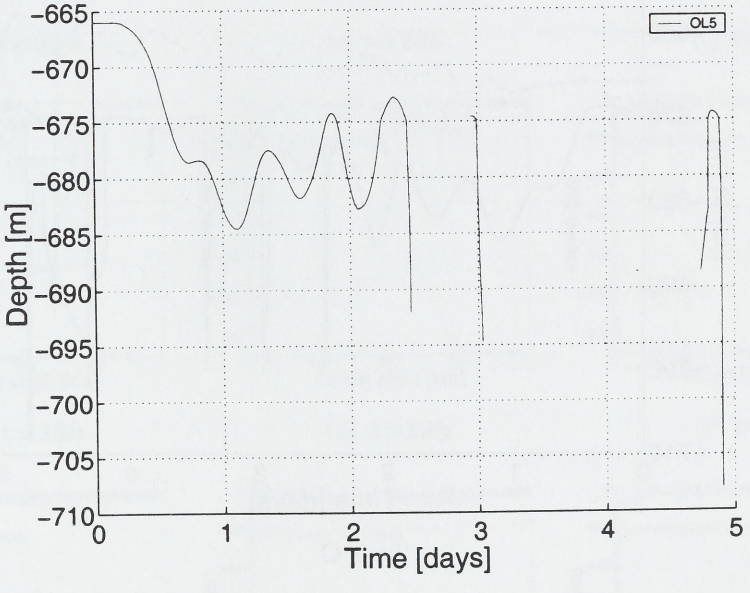

(b) 0°C

Figure 10: **The vertical displacements of the depth of the a) 4°C and b) 0°C iso-surfaces for station OL1-OL5 for the Reference experiment.**

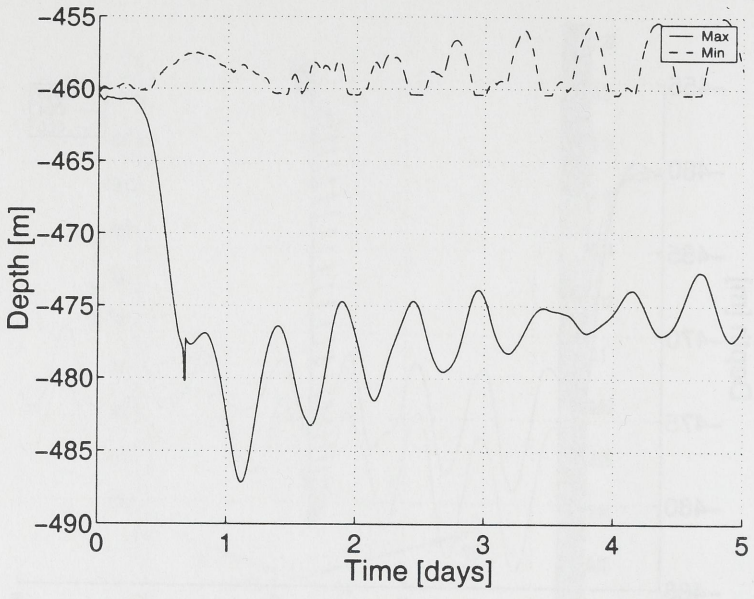

(a) 4°C

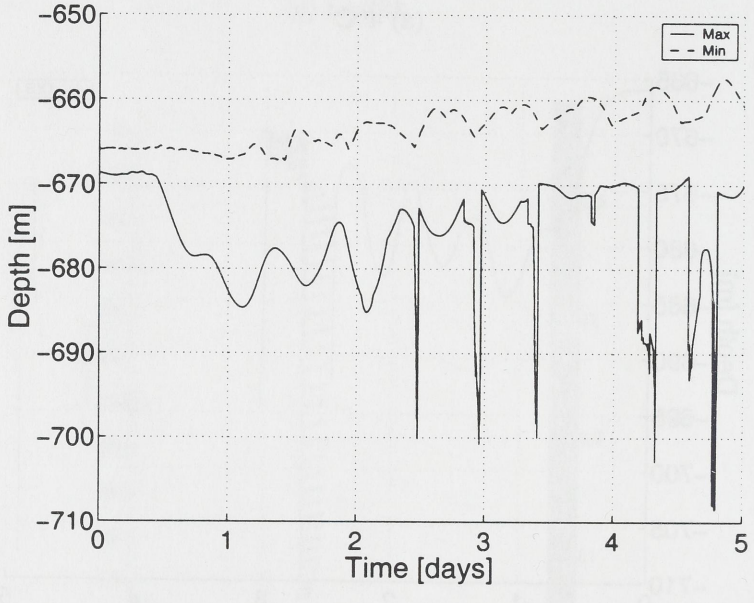

(b) 0°C

Figure 11: **The maximum and minimum of the depths of the a) 4°C and b) 0°C iso-surfaces in the model area for the Reference experiment.**

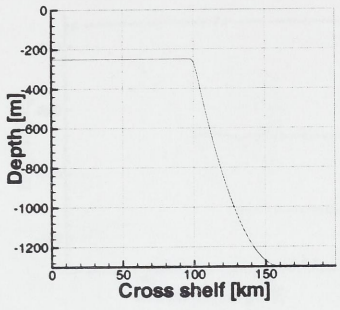

(a) t=0

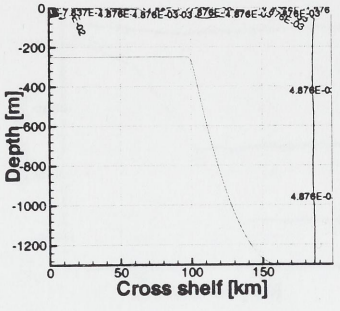

(b) t=12h

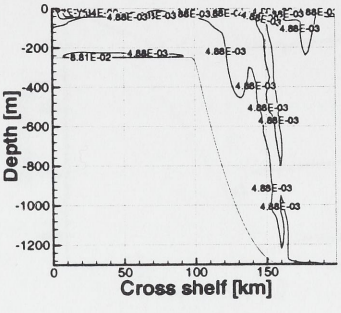

(c) t=24h

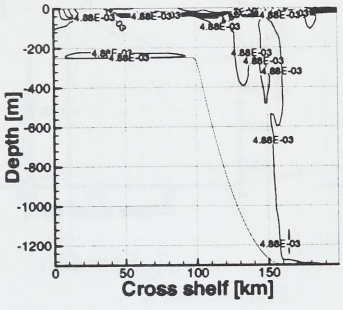

(d) t=25h

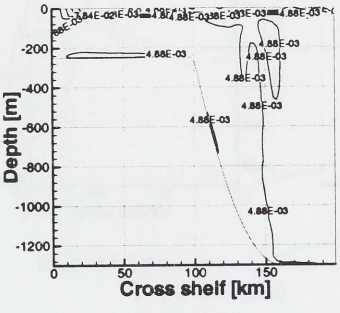

(e) t=26h

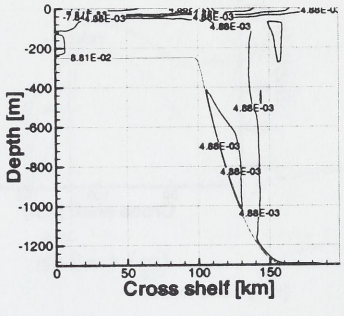

(f) t=27h

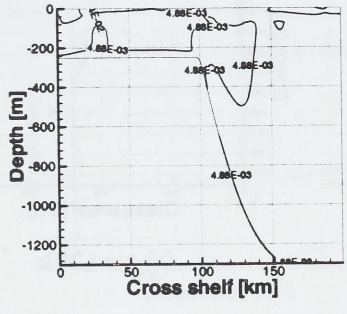

(g) t=28h

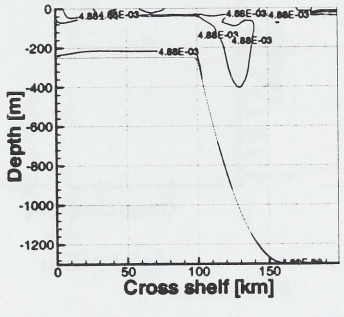

(h) t=29h

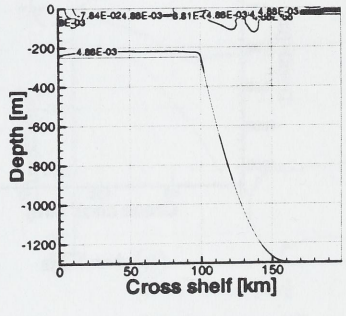

(i) t=30h

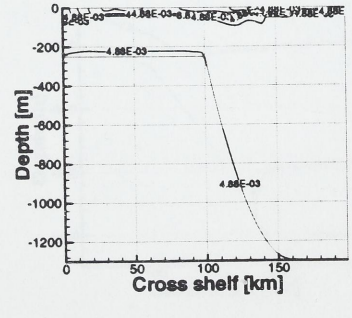

(j) t=31h

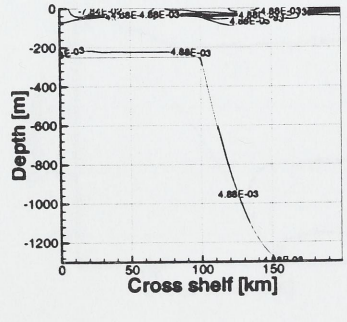

(k) t=32h

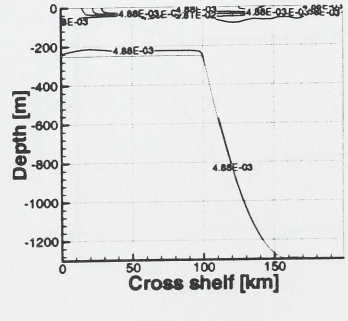

(l) t=33h

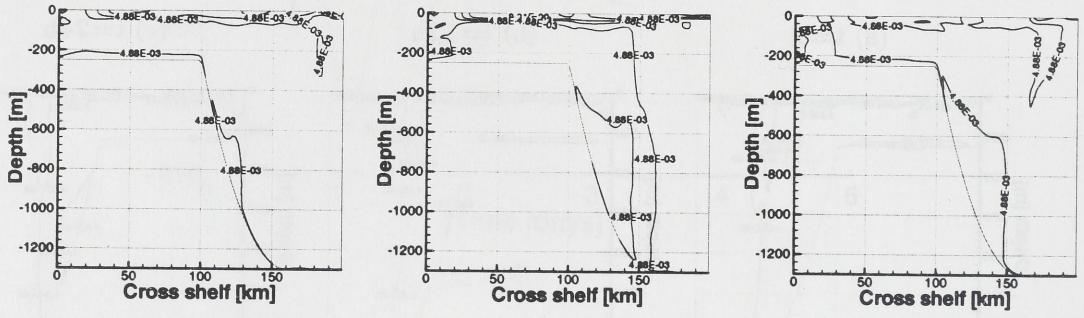

(m) t=34h (n) t=40h (o) t=48h

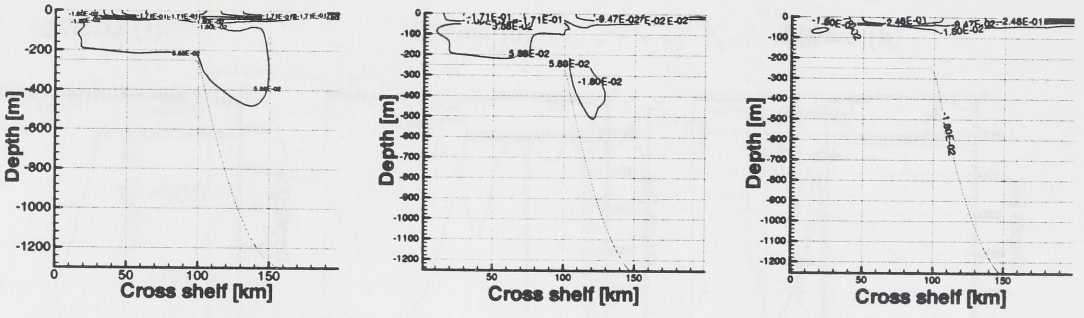

(p) t=72h (q) t=96h (r) t=120h

Figure 12: **Contours of the velocity v in a vertical cross shelf transect for the Reference experiment.**

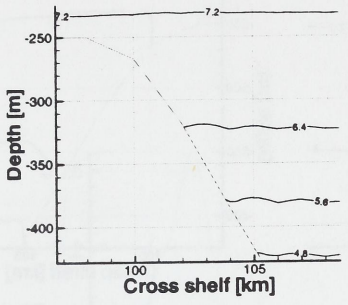

(a) t=0

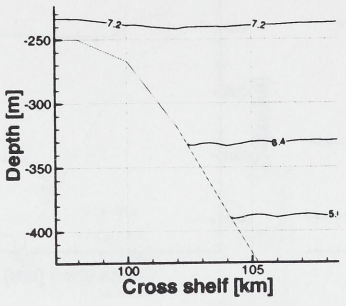

(b) t=12h

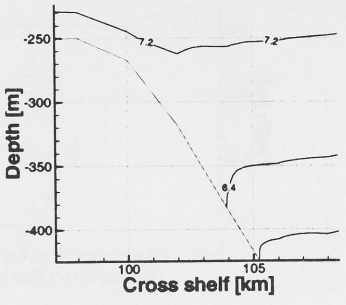

(c) t=24h

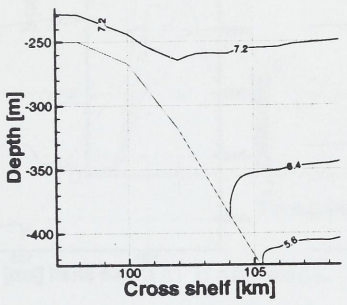

(d) t=25h

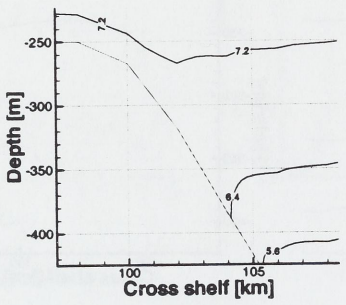

(e) t=26h

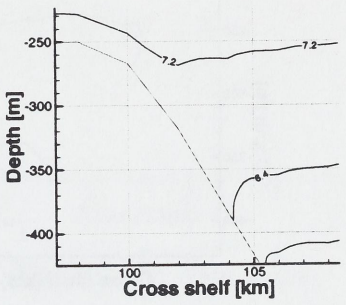

(f) t=27h

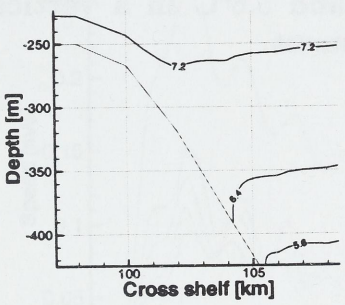

(g) t=28h

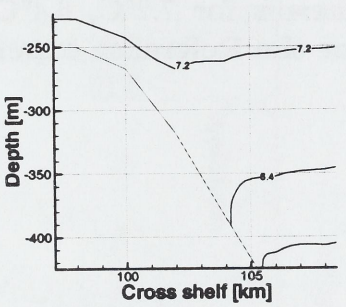

(h) t=29h

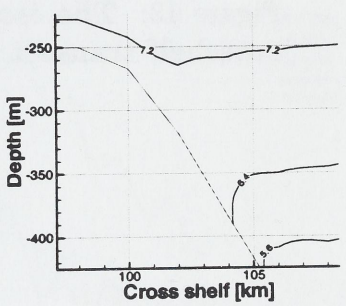

(i) t=30h

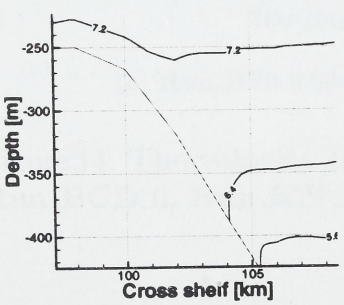

(j) t=31h

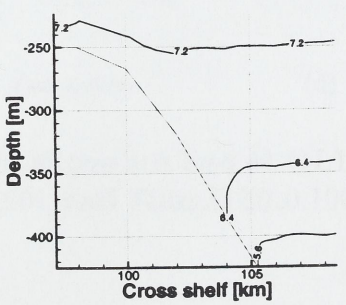

(k) t=32h

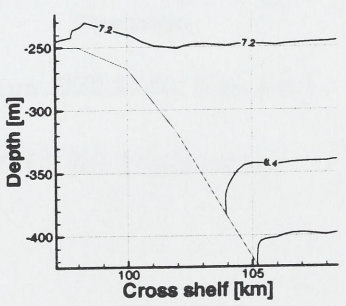

(l) t=33h

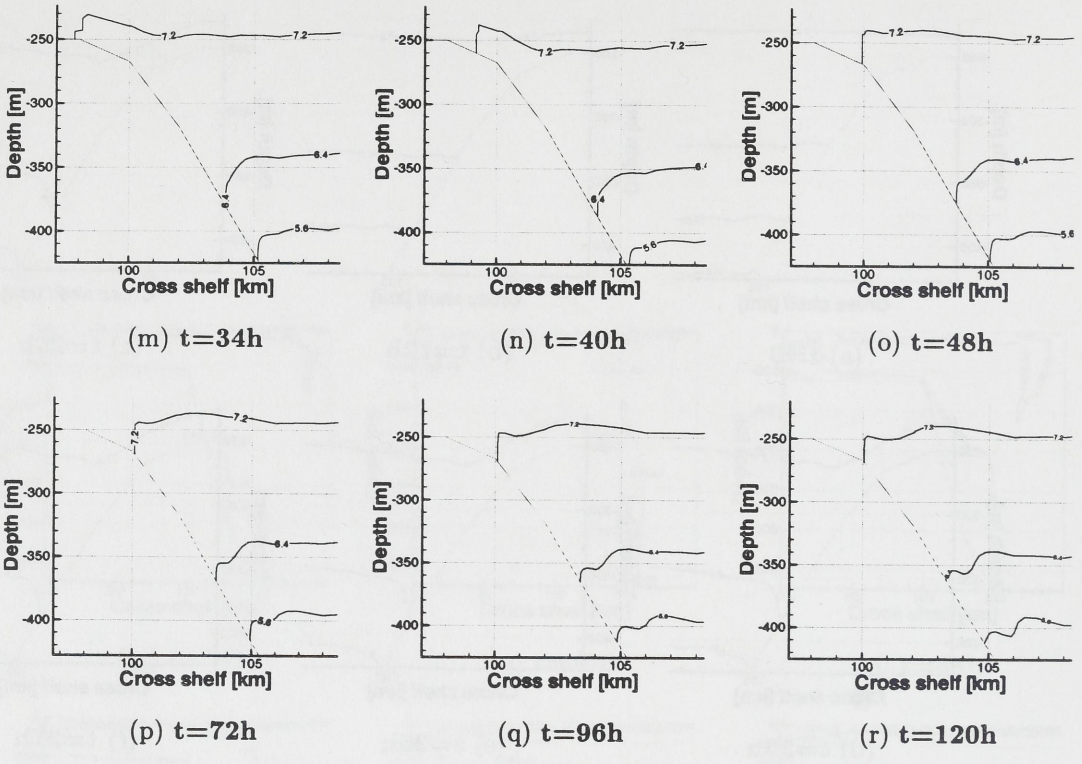

(m) t=34h (n) t=40h (o) t=48h

(p) t=72h (q) t=96h (r) t=120h

Figure 13: **The isotherms for 7.2°C, 6.4°C and 5.6°C in a vertical crosshelf transect for the Reference experiment.**

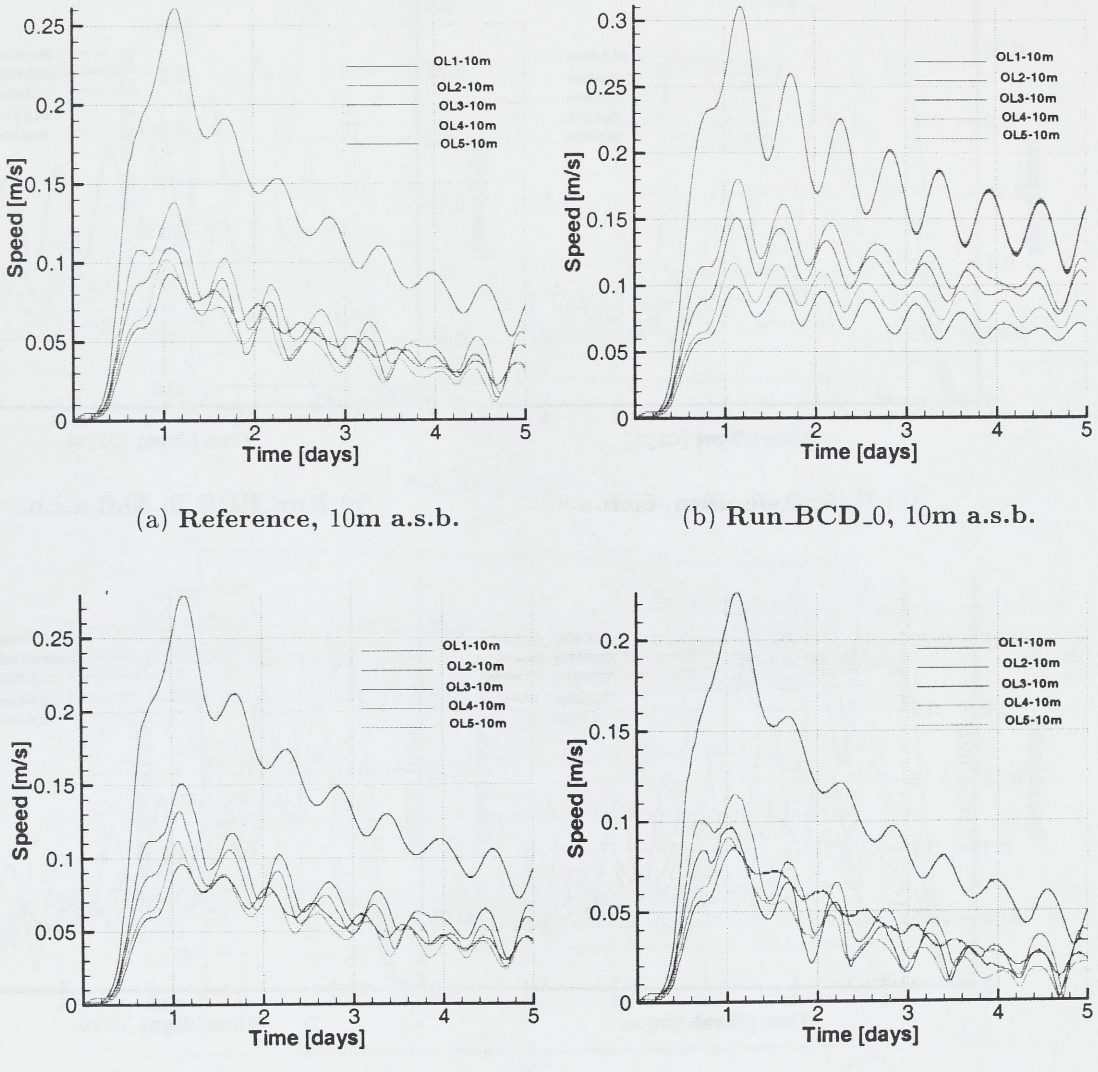

(a) **Reference, 10m a.s.b.**

(b) **Run_BCD_0, 10m a.s.b.**

(c) **Run_BZ0_0.001, 10m a.s.b.**

(d) **Run_BZ0_0.100, 10m a.s.b.**

Figure 14: **The velocity 10m above sea bed at OL1-OL5 for Reference, Run_BCD_0, Run_BZ0_0.001 and Run_BZ0_0.100.**

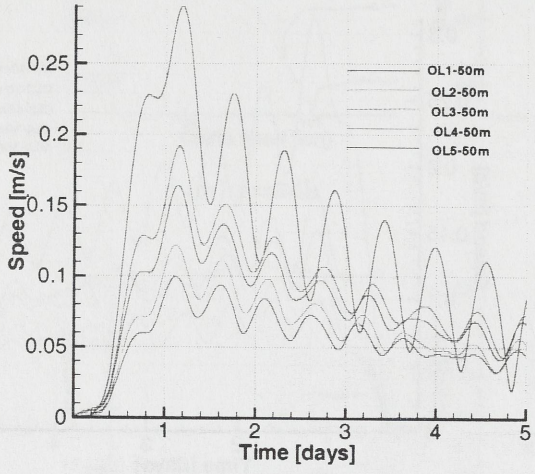

(a) **Reference, 50m a.s.b.**

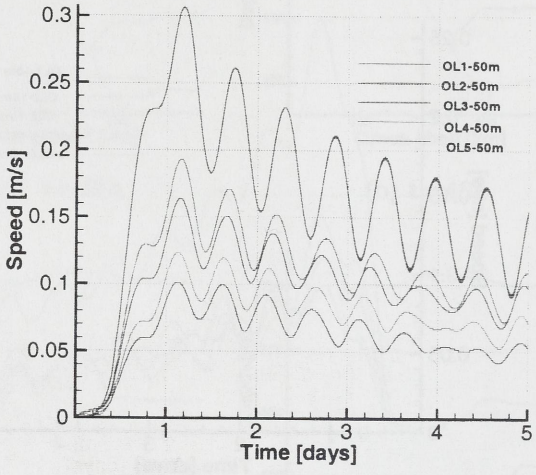

(b) **Run_BCD_0, 50m a.s.b.**

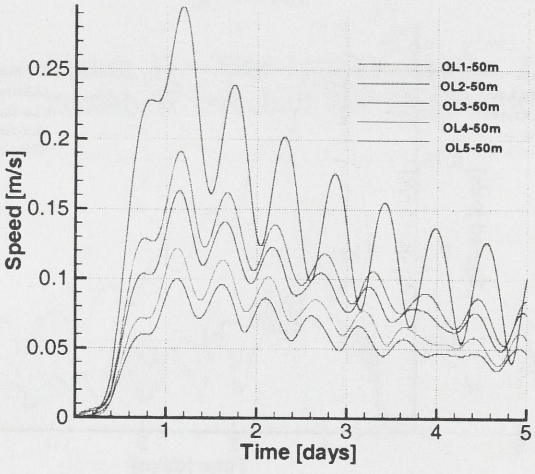

(c) **Run_BZ0_0.001, 50m a.s.b.**

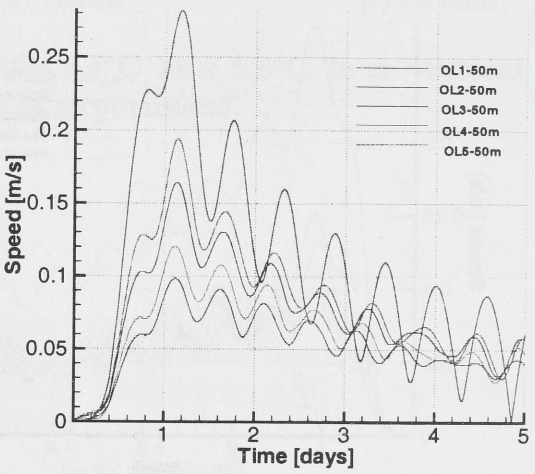

(d) **Run_BZ0_0.100, 50m a.s.b.**

Figure 15: **The velocity 50m above sea bed at OL1-OL5 for Reference, Run_BCD_0, Run_BZ0_0.001 and Run_BZ0_0.100.**

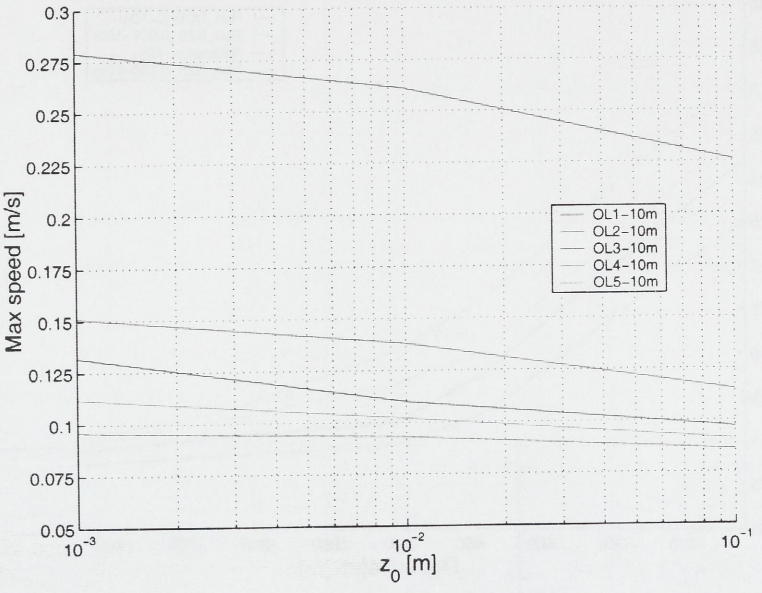

(a) 10m a.s.b.

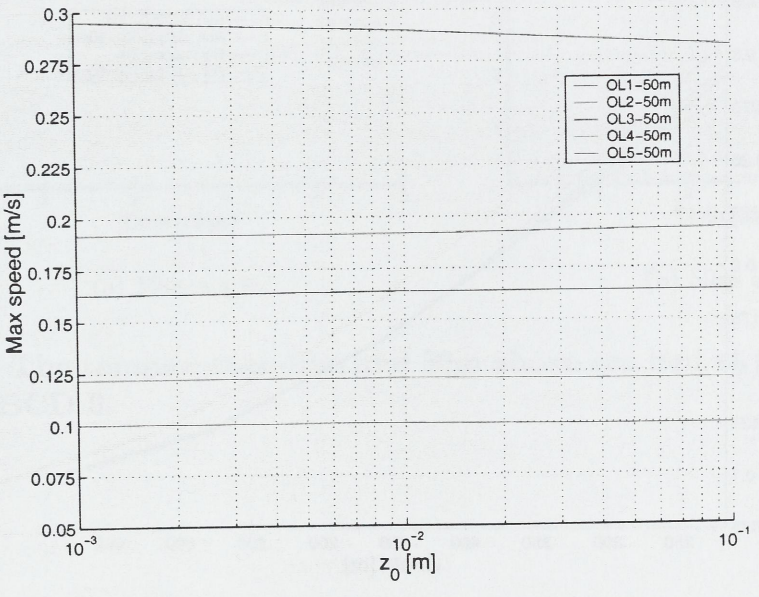

(b) 50m a.s.b.

Figure 16: **Decreasing maximum velocity at OL1-OL5 with increasing values of the bottom roughness parameter. In a) 10m and b) 50m above sea bed. A logarithmic scale is used for the x-axis.**

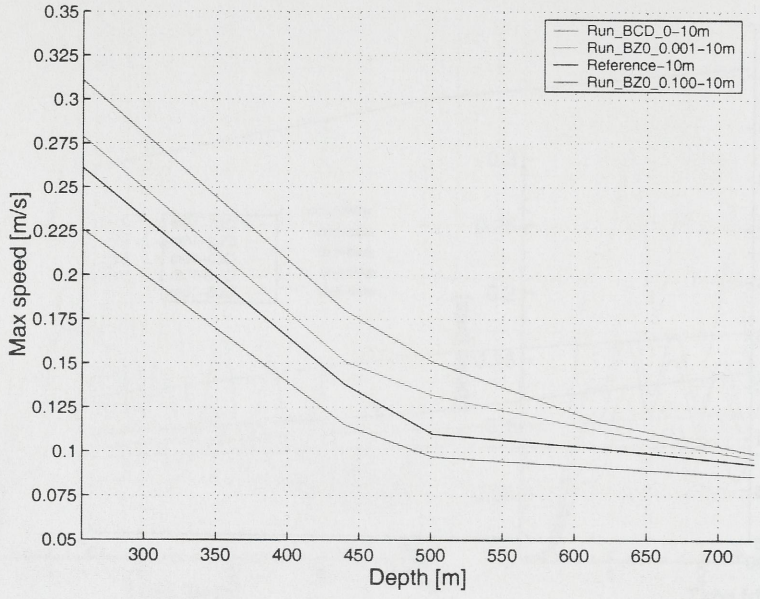

(a) 10m a.s.b.

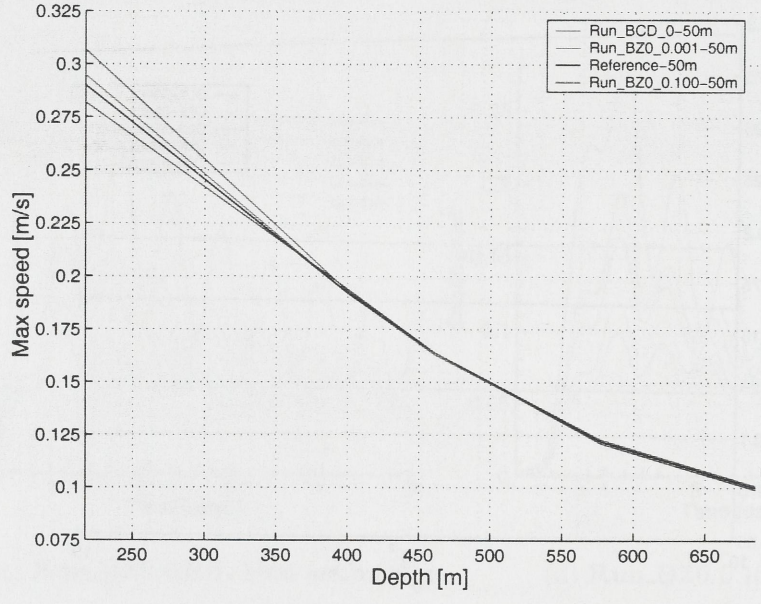

(b) 50m a.s.b.

Figure 17: **Increasing maximum velocity with depth at OL1-OL5 for the Run_BZ and Reference experiments. In a) 10m and in b) 50m above sea bed.**

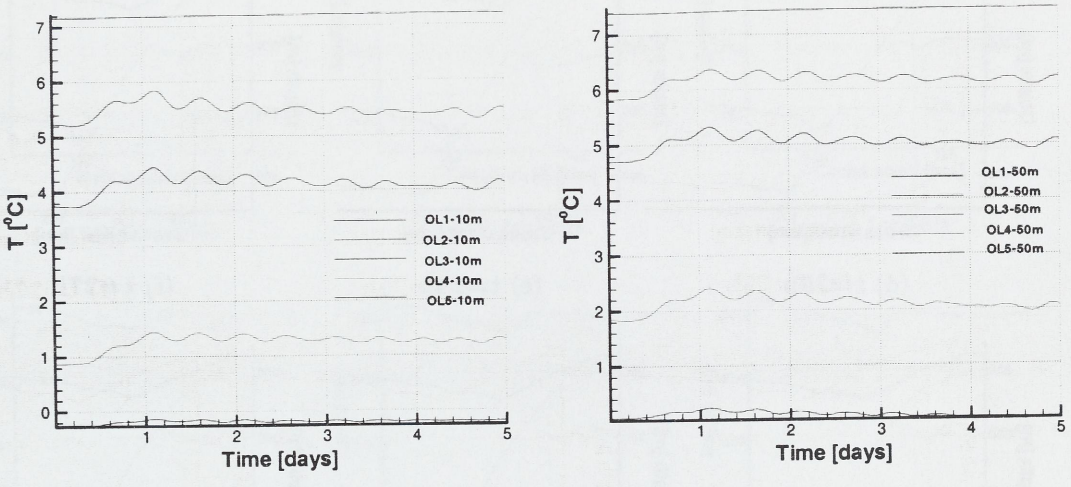

(a) 10m a.s.b.

(b) 50m a.s.b.

Figure 18: **The temperature 10m and 50m above sea bed at OL1-OL5 for Run_BCD_0.**

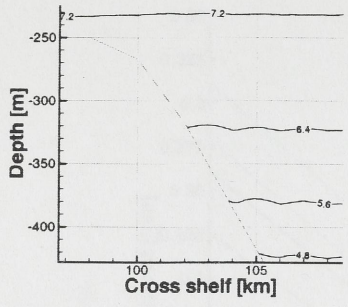

(a) t=0

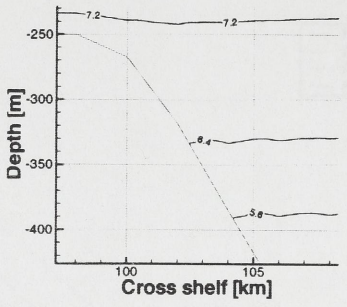

(b) t=12h

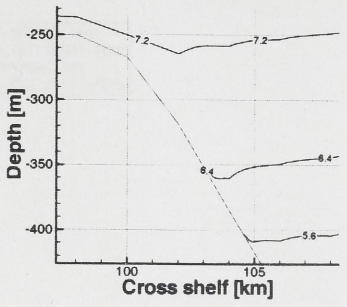

(c) t=24h

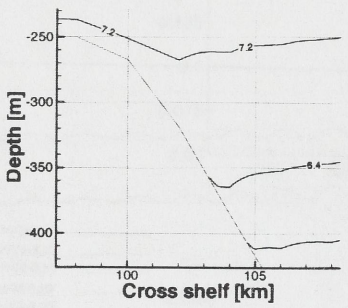

(d) t=25h

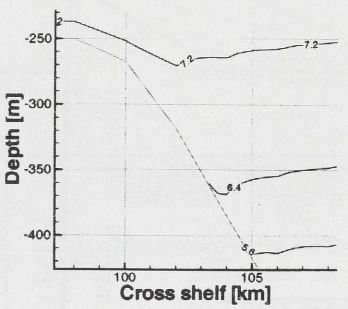

(e) t=26h

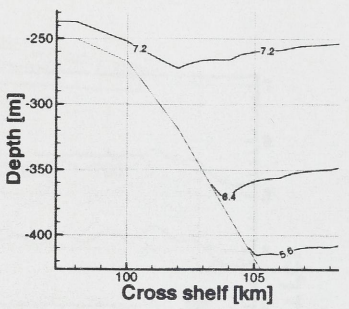

(f) t=27h

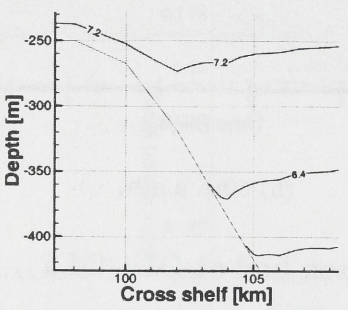

(g) t=28h

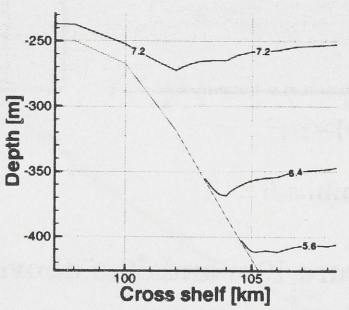

(h) t=29h

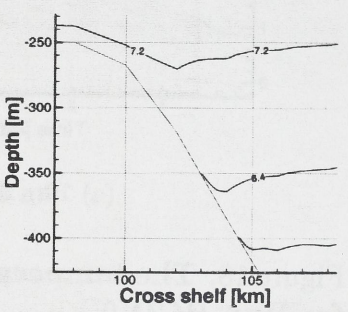

(i) t=30h

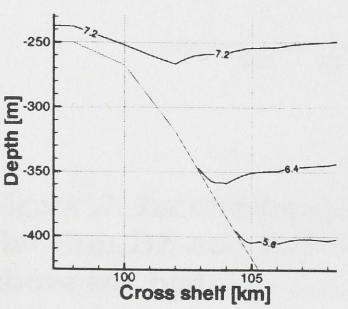

(j) t=31h

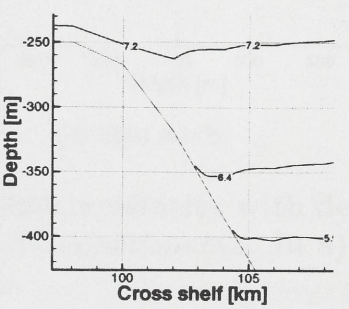

(k) t=32h

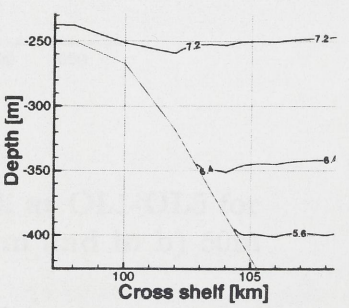

(l) t=33h

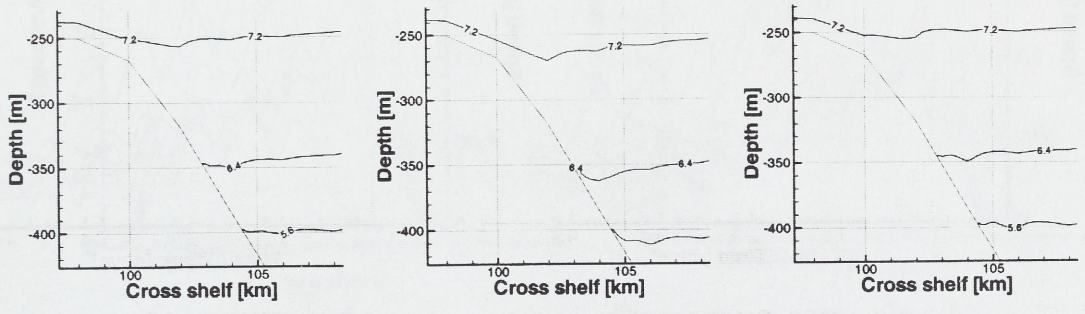

(m) t=34h (n) t=40h (o) t=48h

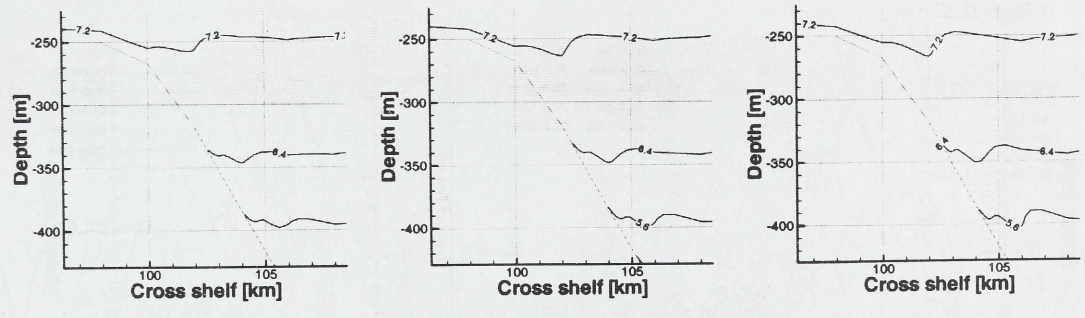

(p) t=72h (q) t=96h (r) t=120h

Figure 19: **The isotherms for 7.2°C, 6.4°C and 5.6°C in a vertical cross shelf transect for Run_BCD_0.**

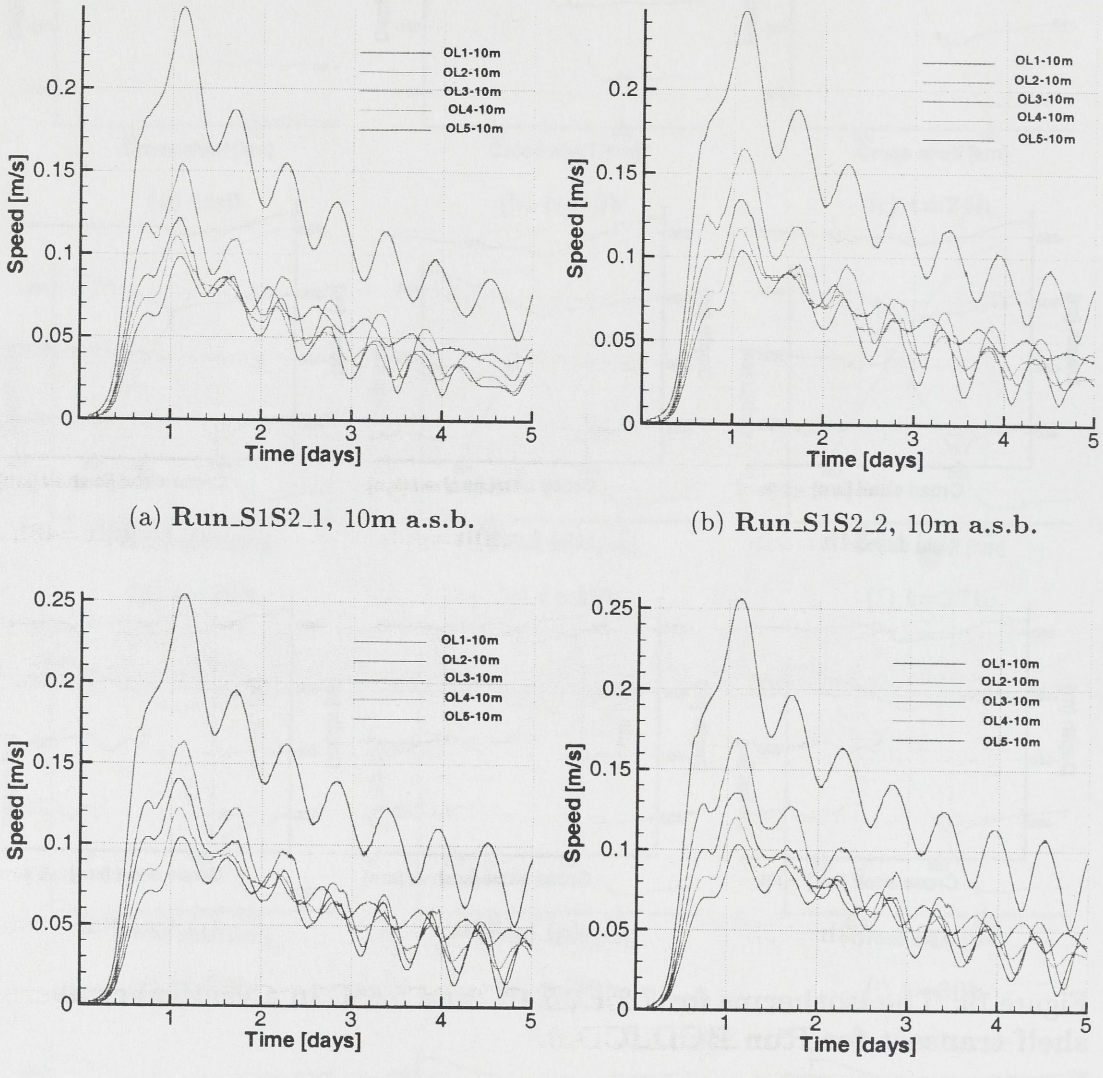

(a) **Run_S1S2_1, 10m a.s.b.**

(b) **Run_S1S2_2, 10m a.s.b.**

(c) **Run_S1S2_3, 10m a.s.b.**

(d) **Run_S1S2_4, 10m a.s.b.**

Figure 20: **The velocity 10m above sea bed at OL1-OL5 for Run_S1S2_1, Run_S1S2_2, Run_S1S2_3 and Run_S1S2_4.**

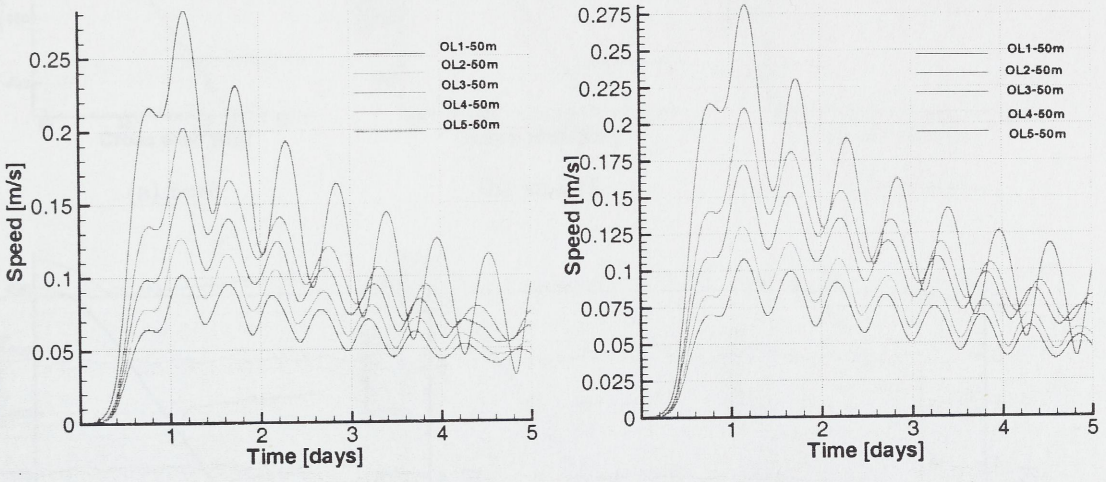

(a) **Run_S1S2_1, 50m a.s.b.**

(b) **Run_S1S2_2, 50m a.s.b.**

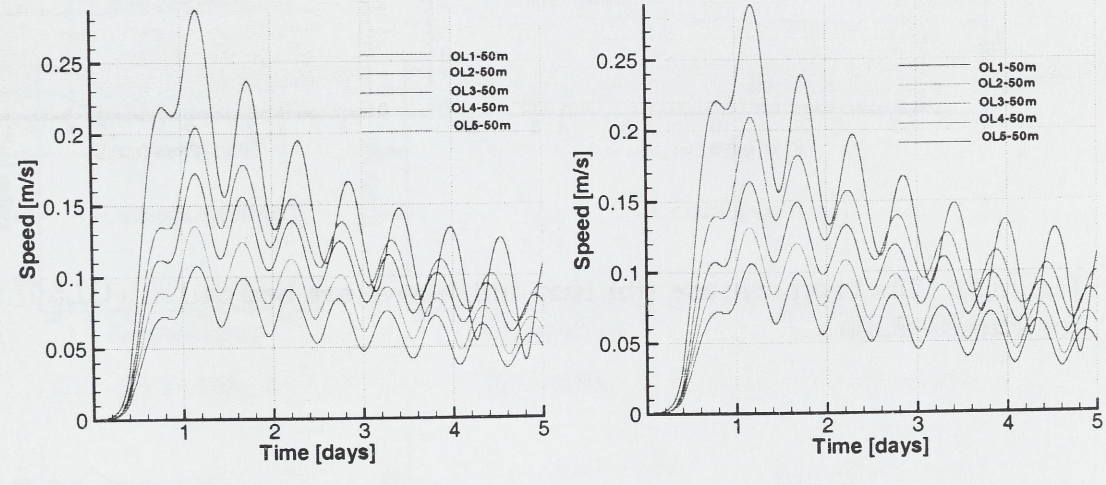

(c) **Run_S1S2_3, 50m a.s.b.**

(d) **Run_S1S2_4, 50m a.s.b.**

Figure 21: **The velocity 50m above sea bed at OL1-OL5 for Run_S1S2_1, Run_S1S2_2, Run_S1S2_3 and Run_S1S2_4.**

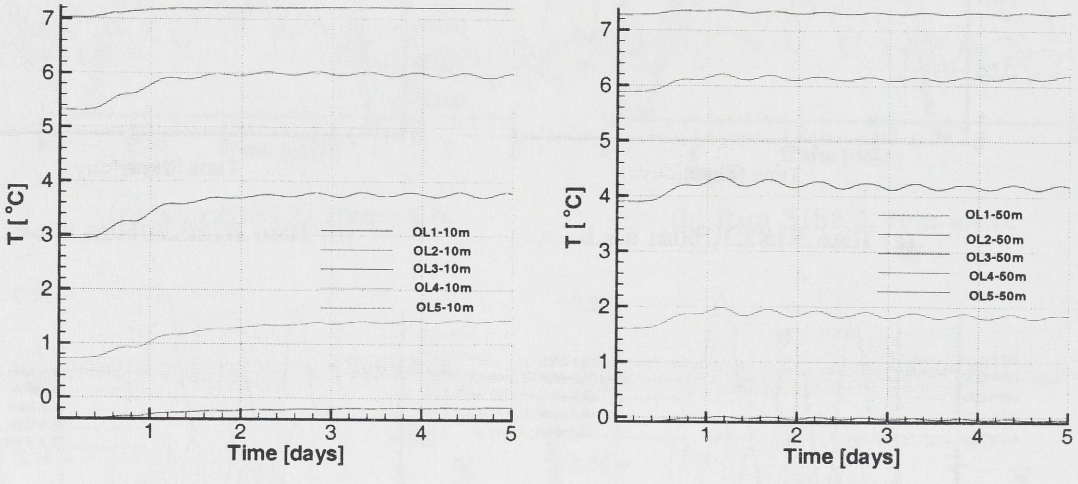

(a) 10m a.s.b.

(b) 50m a.s.b.

Figure 22: **The temperature 10m and 50m above sea bed at OL1-OL5 for Run_S1S2_4.**

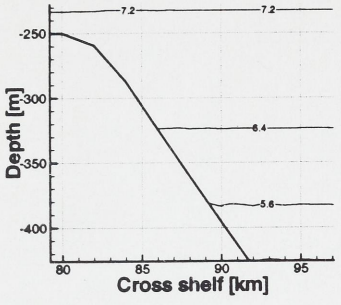

(a) t=0

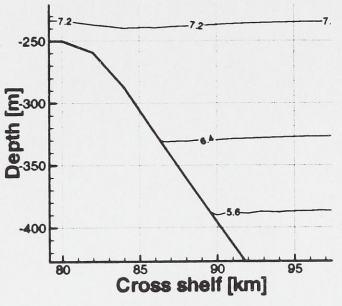

(b) t=12h

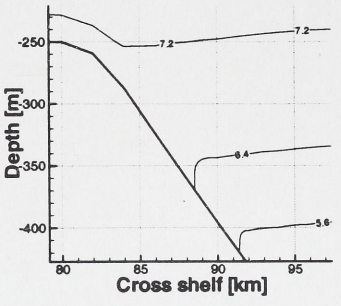

(c) t=24h

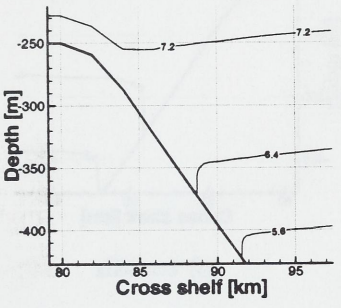

(d) t=25h

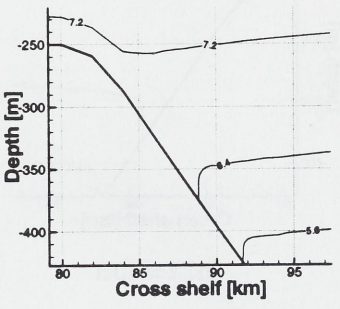

(e) t=26h

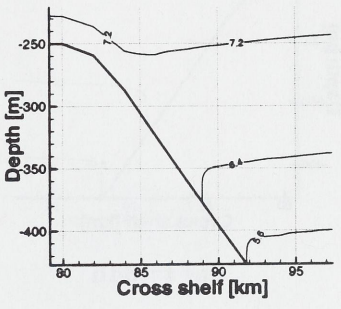

(f) t=27h

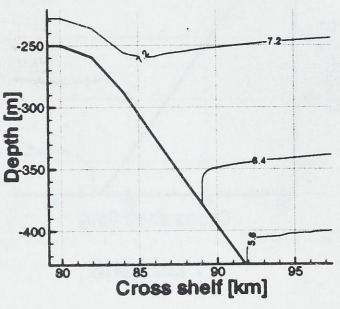

(g) t=28h

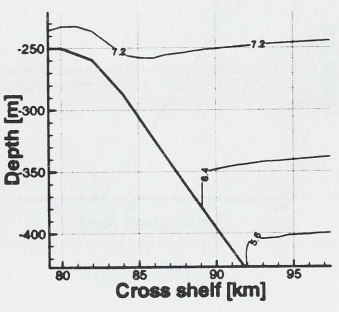

(h) t=29h

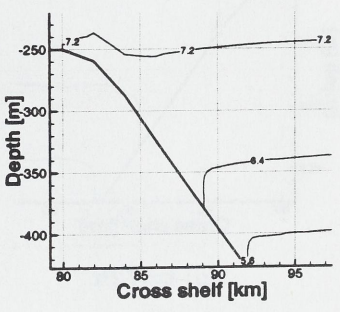

(i) t=30h

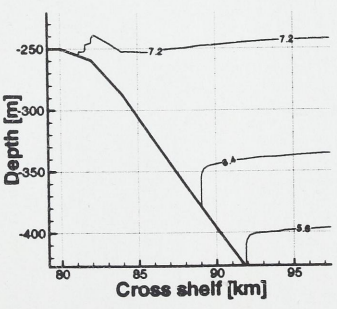

(j) t=31h

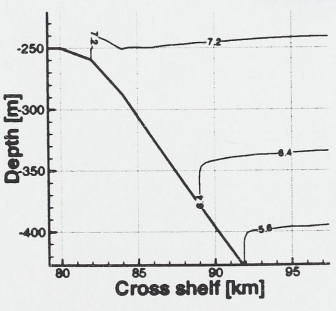

(k) t=32h

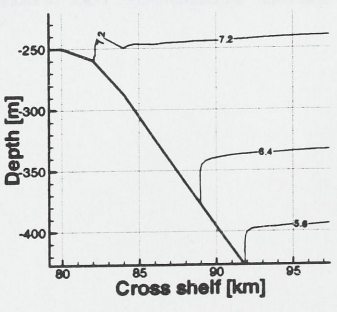

(l) t=33h

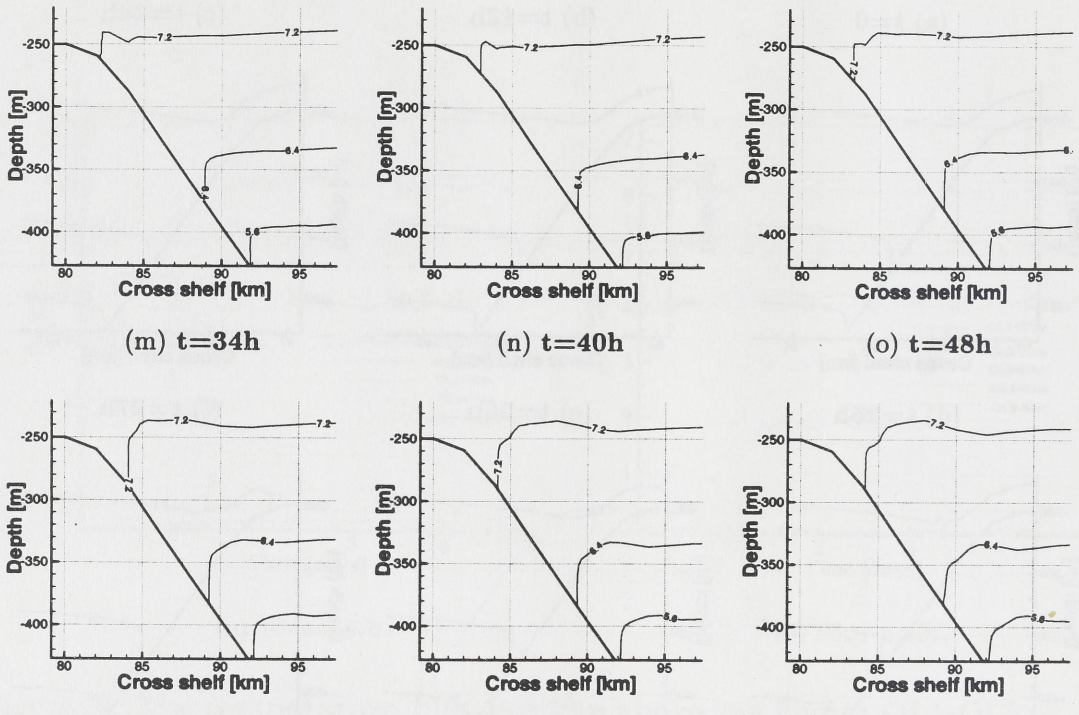

(m) t=34h (n) t=40h (o) t=48h

(p) t=72h (q) t=96h (r) t=120h

Figure 23: **The isotherms for 7.2°C,6.4°C and 5.6°C in a vertical cross shelf transect for Run_S1S2_4.**